

†Retired from Ministerio de Medio Ambiente y Recursos Naturales, San Salvador, El Salvador

Key Points:

- Distributed deformation once extended across Guatemala and into Honduras and has localized into the Guatemala City graben region over time
- The Guatemala City graben region is the current North America, Central American Forearc, and Caribbean plate triple junction
- Faulting in western Guatemala, representing internal deformation of the Caribbean plate, ceased in an eastward direction over the past ~4 Ma

Supporting Information:

Supporting Information may be found in the online version of this article.

Correspondence to:

B. Garnier,
bridget.garnier@me.com


Citation:

Garnier, B., Tikoff, B., Flores, O., Jicha, B., DeMets, C., Cosenza-Murales, B., et al. (2022). Deformation in western Guatemala associated with the NAFCA (North America-Central American Forearc-Caribbean) triple junction: Neotectonic strain localization into the Guatemala City graben. *Tectonics*, 41, e2021TC006739. <https://doi.org/10.1029/2021TC006739>

Received 26 JAN 2021

Accepted 7 JAN 2022

Deformation in Western Guatemala Associated With the NAFCA (North America-Central American Forearc-Caribbean) Triple Junction: Neotectonic Strain Localization Into the Guatemala City Graben

Bridget Garnier¹ , Basil Tikoff¹, Omar Flores², Brian Jicha¹ , Charles DeMets¹ , Beatriz Cosenza-Murales^{1,3} , Walter Hernandez[†], and David Greene⁴

¹Department of Geoscience, University of Wisconsin-Madison, Madison, WI, USA, ²Centro de Estudios Superiores de Energía y Minas, Edificio T-1, Universidad de San Carlos de Guatemala, Ciudad Universitaria, Guatemala City, Guatemala, ³Instituto de Investigación en Ciencias Físicas y Matemáticas, Escuela de Ciencias Físicas y Matemáticas, Universidad de San Carlos de Guatemala, Ciudad Universitaria, Guatemala City, Guatemala, ⁴Department of Earth and Environmental Sciences, Denison University, Granville, OH, USA

Abstract Recent structural and geodetic data define the Guatemala City graben region as the continental triple junction between the North American plate, Caribbean plate, and the Central American Forearc sliver. We present minor fault analysis, geochronological and geochemical analyses, and newly updated GPS velocities in western Guatemala, west of the Guatemala City graben, to characterize the magnitude and timing of extensional deformation in this poorly understood area. Elongations estimated from fault data are parallel (~east-west) and perpendicular to the Polochic-Motagua fault system to the north, similar to geodetically measured active deformation observed east of the Guatemala City graben. Four new ⁴⁰Ar/³⁹Ar dates and correlation of tephra deposits suggest that faulting was active during the Pliocene, but ceased eastward toward the Guatemala City graben over time. From west to east, fault cessation occurred before the deposition of the Los Chocoyos ash (75 ka) and E tephra (51 ka). Faulting just west of the Guatemala City graben appears to be active, where a major fault cuts the most recent Amatitlán tephra. Based on this data, we propose a time-progressive strain model for deformation related to North America-Caribbean plate interactions, whereby distributed elongation of the westernmost Caribbean plate occurred during the Pliocene but localized mostly within the Guatemala City graben and nearby faults during the Pleistocene. Our model supports that: (a) The Guatemala City graben is effectively the western limit of the Caribbean plate; and (b) Western Guatemala, which was the trailing edge of the Caribbean plate, has been transferred to the forearc region.

1. Introduction

One implication of the plate tectonics paradigm is the existence of triple junctions, where the boundaries between three plates intersect (Morgan, 1968). McKenzie and Morgan (1969) first proposed methods to determine whether the geometry of a triple junction will remain stable or change over time based on the type and geometry of the intersecting plate boundaries (also see Cronin, 1992; York, 1973). Their work has proved useful for understanding the kinematics and geometric evolutions of most oceanic triple junctions, where the intersecting plate boundaries and plate kinematics are both well defined. On the continents, where active deformation is often distributed over wide areas, identifying triple junctions and how they evolve with time has proved more challenging.

In Central America, studies have proposed the existence of a triple junction between the North America, Caribbean, and Cocos plates (Figure 1; Álvarez-Gómez et al., 2008; Authemayou et al., 2011; Franco et al., 2012; Lyon-Caen et al., 2006; Phipps Morgan et al., 2008; Plafker, 1976). Following the February 4, 1976 Motagua fault earthquake ($M_w = 7.5$), which killed or injured 2% of the population of Guatemala and left another 20% of the population homeless, Plafker (1976) outlined several models for the plate boundary geometry and associated deformation of this system. These early models include the existence of a triple junction offshore from Guatemala or Mexico, where the sinistral Polochic and Motagua strike-slip faults between the North America and Caribbean plates should intersect the Middle America trench and subducting Cocos plate (Figure 1; Burkart, 1978, 1983; Muehlberger & Ritchie, 1975; Plafker, 1976). With offshore triple junction models, continued movement of the continental plates in opposing directions would offset the trench. As the trench is continuous and not offset,

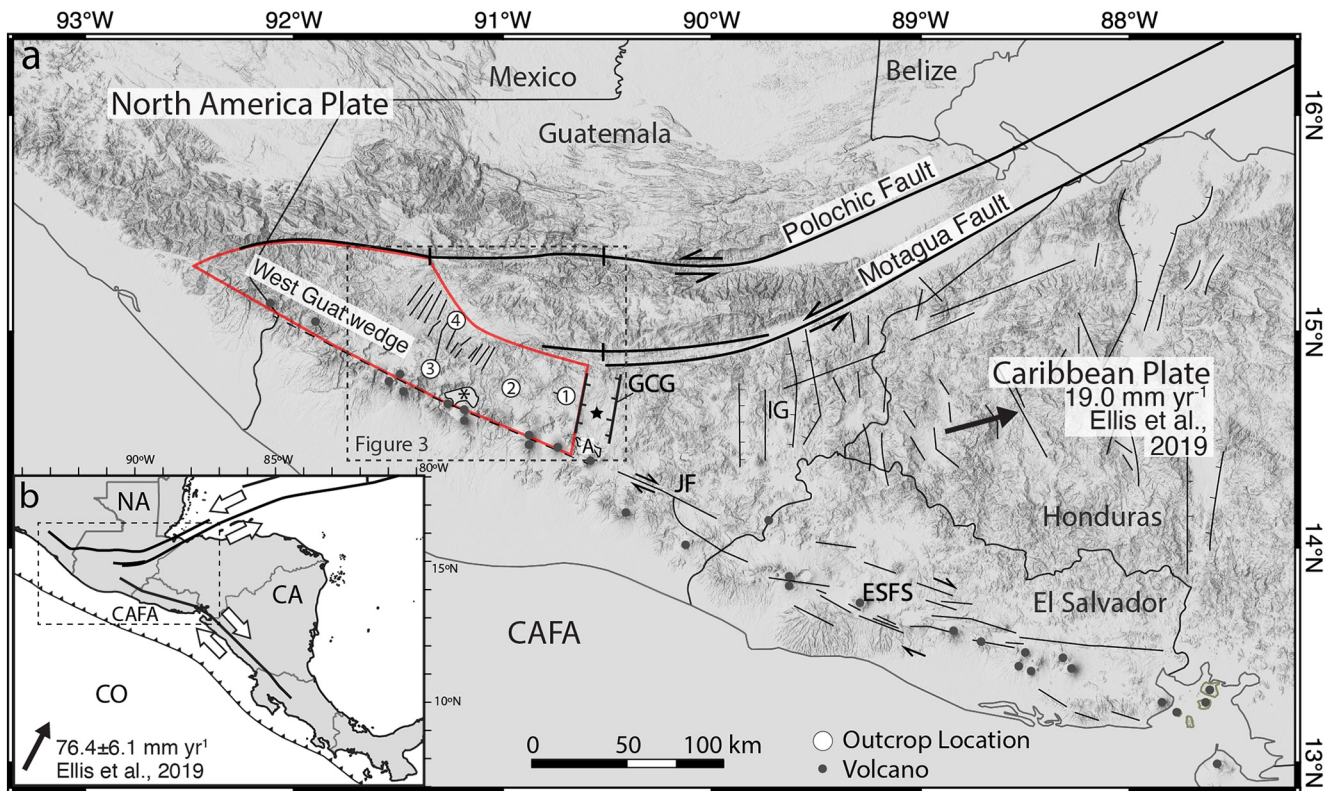


Figure 1. (a) Annotated DEM of North America, Caribbean, Central American Forearc (CAFA), and Cocos plate interactions in north Central America. The major structures are identified, along with the Guatemala City graben (GCG) containing Guatemala City (star), the Ipala graben (IG), the Jalpatagua fault (JF), the El Salvador fault system (ESFS), and the Central American Forearc (CAFA). Numbered, white circles show location of study areas: Xenacoj (1), Tecpan (2), Nahualá (3), and Ilotenango (4). Location of the Atitlán caldera is shown with a *, between locations 3 and 2. Amatitlán caldera is marked with an A on the southern end of the Guatemala City graben. Mapped faults in Honduras are from Rogers (2002). The west Guatemalan wedge is outlined in red, with the Polochic fault, Guatemala City graben, and the volcanic arc as the major bounding structures. Gray dashed box outlines the area presented in Figure 3. (b) Inset map of major plate boundaries and relative motion in Central America. Major plates shown are CO, Cocos plate; NA, North America plate; CA, Caribbean plate; and the CAFA, Central American Forearc. Solid black lines indicate the Polochic-Motagua fault system between the NA and CA plates and the forearc boundary between the CA and CAFA plates. White arrows indicate relative motions across these two boundaries. Motions of the Caribbean and Cocos plates are from Ellis et al. (2019) and are in relation to a stable North American plate.

subsequent models suggest that the Caribbean and North America plates meet at a diffuse onshore triple junction in western Guatemala, where the Polochic-Motagua fault system meets the volcanic arc (e.g., Álvarez-Gómez et al., 2019; Andreani & Gloaguen, 2016; Authemayou et al., 2011; Franco et al., 2012; Gordon & Muehlberger, 1994; Guzmán-Speziale et al., 1989; Lyon-Caen et al., 2006; Phipps Morgan et al., 2008). The offshore and onshore triple junction models also suggest extensional deformation within the Caribbean plate as it moves eastward in relation to the North America plate.

The introduction of geodesy as a means to define the regional crustal velocity field enabled studies of the seismic cycles of the major active faults and the related regional deformation, furthering development of the tectonic models. Lyon-Caen et al. (2006) focused on the seismically active Polochic-Motagua fault zone (Figure 1), which accommodates North America-Caribbean plate motion. The velocity field strongly indicates that most, or possibly all, of the motion along the Polochic-Motagua fault zone is transferred northward onto reverse faults and strike-slip faults in southern Mexico and southward to north-striking grabens in western Honduras and southern Guatemala (Lyon-Caen et al., 2006). Subsequent GPS measurements across the Salvadoran and Guatemalan volcanic arcs (Alvarado et al., 2011; Correa-Mora et al., 2009; Franco et al., 2012; Kobayashi et al., 2014; Staller et al., 2016) show that the Central American Forearc (CAFA) translates rapidly westward as a rigid or semi-rigid sliver (Figure 1). Faults along the volcanic arc accommodate this forearc motion and nearly intersect the Polochic-Motagua fault zone to the west, near the Mexico-Guatemala border. Recent work by Ellis et al. (2018, 2019) increases the geodetic resolution of northern Central America, including western Guatemala which previously

had very few GPS sites. The available geodetic measurements indicate that the CAFA west of the Guatemala City graben and other areas of western Guatemala move nearly with the North America plate, with most deformation focused farther to the east in central and eastern Guatemala and Honduras.

Based on geodetic and structural data of the last two decades, proposed models for northern Central American plate interactions need to address the broad continental deformation north and south of the sinistral Polochic-Motagua faults of Guatemala, the role of the CAFA, and possible pinning of the CAFA to the North America plate in western Guatemala. The most recent models continue to suggest a diffuse onshore triple junction in western Guatemala, but propose that the tectonic system evolves as a southeast-directed, migrating triple junction. Authemayou et al. (2011) introduced a “zipper” model, which proposes a progressive development for deformation in Guatemala whereby the CAFA progressively fuses to the North America plate as the Caribbean plate and a triple junction move eastward (e.g., Álvarez-Gómez et al., 2019; Andreani & Gloaguen, 2016; Franco et al., 2012). Further data and modeling by Álvarez-Gómez et al. (2019) produced a kinematic model that supports the zipper model with additional focus on the CAFA. They propose that the forearc is pulled to the northwest by the North America plate, but is also pushed at the other end by the collision of the Cocos Ridge in Costa Rica, like a pull-push train (Kobayashi et al., 2014; LaFemina et al., 2009). Additionally, their model indicates that the CAFA undergoes slight counterclockwise rotation at the northwestern end to parallel North America velocity directions. Within this model, western Guatemala is the next region to be affected by “zippering” of the CAFA to North America. However, with the latest GPS data from Ellis et al. (2018, 2019), deformation in western Guatemala is now shown to be fairly inactive and it is unclear if this region still belongs to the extending Caribbean plate.

In this contribution, we document the timing and deformation of fault systems in western Guatemala, in an area west of the Guatemala City graben, to see how the deformation compares to previously proposed tectonic models, including the most recent zipper model. Our estimates of timing of fault activity are based on stratigraphic correlation and four new $^{40}\text{Ar}/^{39}\text{Ar}$ dates, with each one constraining fault movement related to deformation between the Polochic-Motagua fault system and the volcanic arc-CAFA. Structural observations from a new, well-exposed outcrop (Xenacoj) just west of the Guatemala City graben are used to understand deformation immediately west of the Guatemala City graben. A regional GPS velocity field derived from 1993 to 2017 data from Ellis et al. (2018, 2019) and updated with more recent data from campaign sites in southern Guatemala and western El Salvador creates the framework for our interpretation (Garnier et al., 2020; LeGrand et al., 2020). Synthesizing this information, we conclude that the structural data agrees with GPS velocity fields that no active deformation is observed in western Guatemala. Fault data and volcanic deposit ages also indicate that deformation in western Guatemala was more distributed in the Pliocene, and is progressively becoming localized in the Guatemala City graben. As a result, we propose a new localizing strain model—the “alicate” (ah-lee-KHAH-tay) model, meaning “pliers” in Spanish—for deformation associated with the North America-Caribbean plate interactions in Central America, in which strain is progressively localized along the terminations of the Motagua and Jalpatagua faults, into the Guatemala City graben region.

2. The Western Guatemala Wedge

Western Guatemala is in close proximity to the continental triple junction, but few structural and geodetic data have been reported from this region, most likely due to safety concerns and sparse, weathered outcrops. This observation is specifically true for an area that we define as the “western Guatemala wedge” (red outline in Figure 1), which is bounded to the north by the Polochic-Motagua fault system, to the south by the volcanic arc, and to the east by the Guatemala City graben. While the wedge shape description is often extended to the east in other studies, any mention of a wedge in this contribution refers to the western Guatemala wedge that stops at the Guatemala City graben.

Williams (1960) was first to geologically characterize western Guatemala and provides broad lithology and structural descriptions for different regions within the western Guatemala wedge. Later work focused on mapping and characterization of the Quaternary tephra stratigraphy across Guatemala (Koch & McLean, 1975) and the volcanic arc and its related deposits, with particular focus on the Atitlán caldera region (Figure 1; Cisneros de León et al., 2021; Clohan & Reynolds, 1977; Drexler et al., 1980; Eggert & Lea, 1978; Holekamp et al., 1978; Hughes, 1978; Newhall, 1987; Rose et al., 1999, 1979, 1981, 1987). These studies mapped and defined the major Quaternary tephra as they extend from the volcanic arc and into the western Guatemala wedge (Figure 2). While

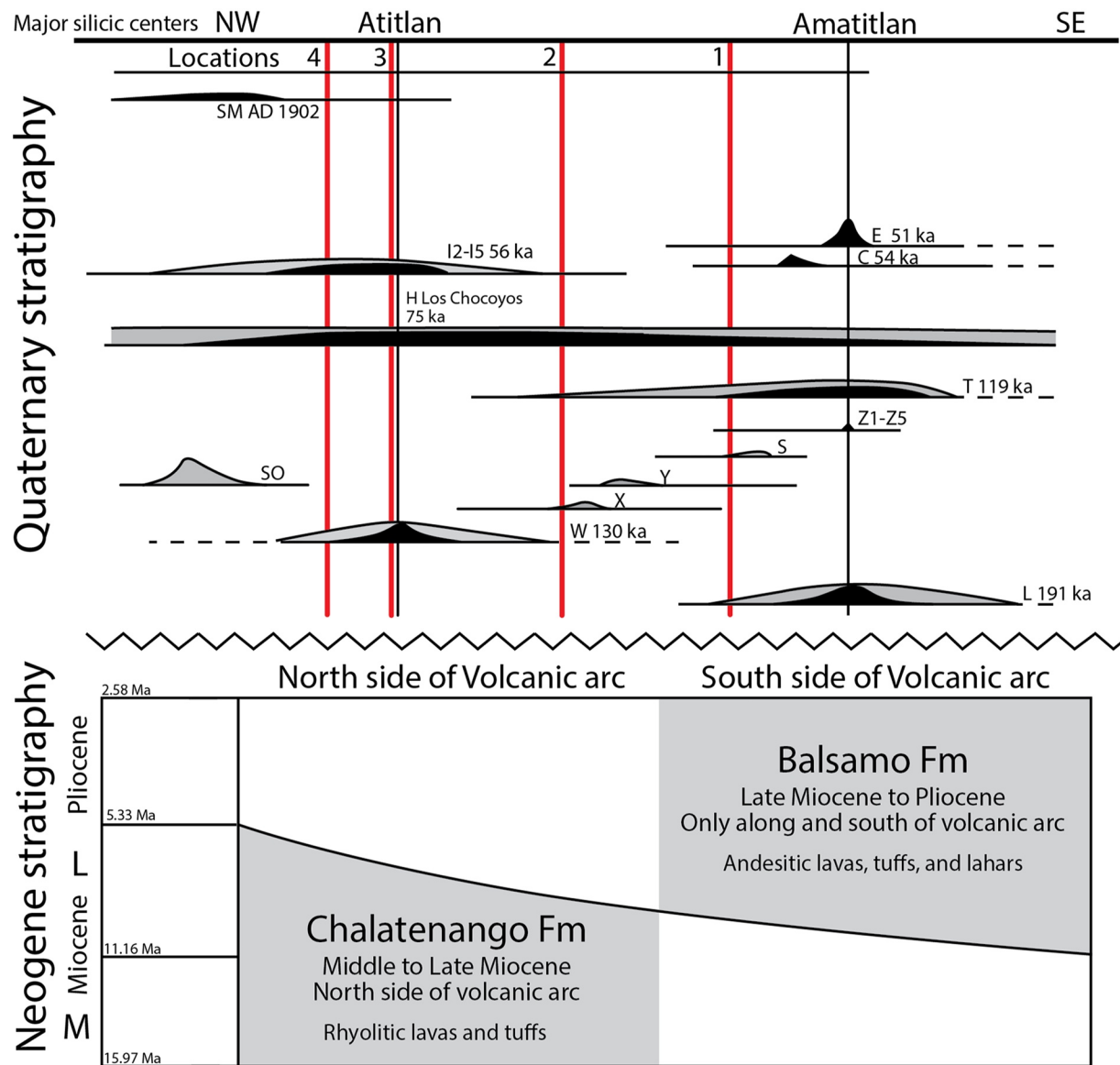


Figure 2. Quaternary and Neogene stratigraphy of southwestern and southcentral Guatemala. Top portion describes the Quaternary stratigraphy (modified from Rose et al., 1999). Vertical red lines indicate the location of outcrops in relation to the major rhyolitic centers, specifying the units that may be (or may not be) observed at each outcrop. Black cones indicate ignimbrite deposits while the lighter gray areas represent the fall out deposits. Tephra labels and possible sources: SM, Santa Maria dacite deposit (Santa Maria volcano), I2-I5, I fall deposits (Atitlán), E, E fall deposit (Amatitlán), C, C fall deposit (Agua volcano), H Los Chocoyos, H fall and ash-flow/Los Chocoyos ash deposit (Atitlán), T, T fall and flow deposit (Amatitlán), Z1-Z5, Z fall deposits (Amatitlán), S, S tephra deposit (Agua volcano), Y, Y tephra deposit (Acatenango or Fuego volcano), SO, Siete Orejas tephra deposit (Siete Orejas volcano), X, X tephra deposit (unknown), W, W fall and flow deposit (Atitlán), L, L fall and flow deposit (Amatitlán). Bottom portion describes the Neogene stratigraphy.

most Quaternary tephras have a Pleistocene age, this term includes even the most recent and smaller volcanic deposits. Quaternary deposits include the Los Chocoyos ash from the Amatitlan calders, which has an assigned age of 75 ± 2 ka based on oxygen-isotope stratigraphy in ocean cores in which it is found (Cisneros de León et al., 2021). The Los Chocoyos ash is the most prominent and wide-spread ash flow tephra across Guatemala and Central America that can exceed 200 m in thickness in basins north of the Atitlán caldera. These thick, blanketing Quaternary tephras limit exposure of the underlying Neogene and older stratigraphy, making it nearly impossible to map individual deposits. Therefore, Neogene and older stratigraphy have been defined as broad units based on a range of deposits that can be observed north and south of the volcanic arc (Figure 2; Reynolds, 1977, 1980; Ritchie, 1975). While structural mapping was completed around volcanic centers along the volcanic arc, similar mapping studies have rarely been done in the wedge north of the volcanic arc.

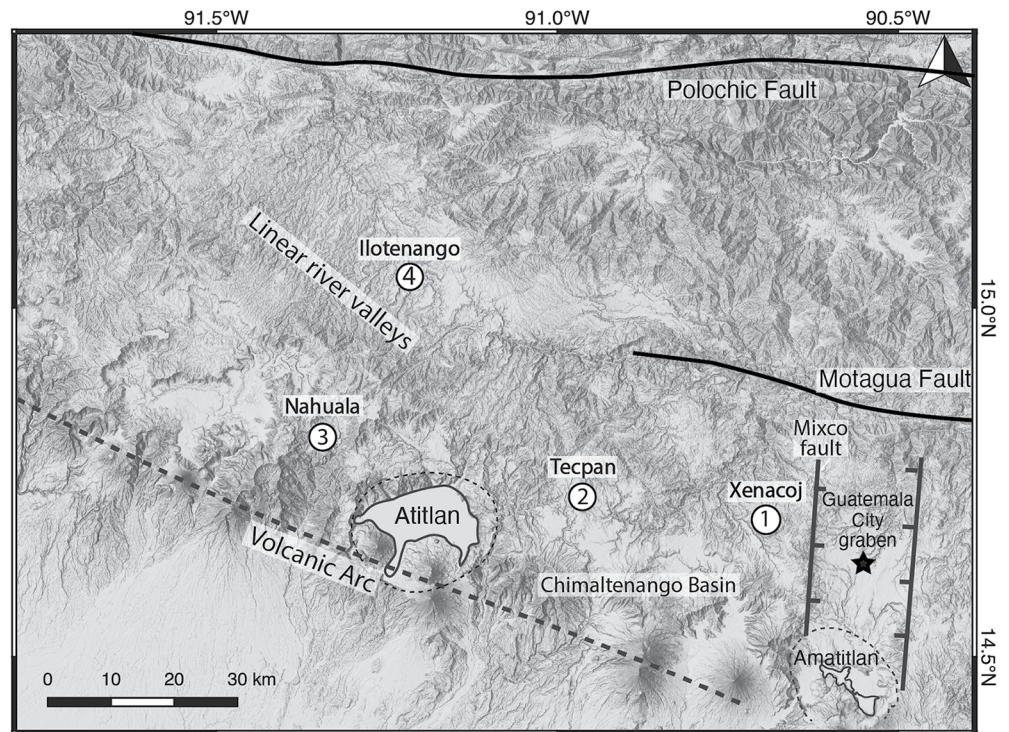


Figure 3. Annotated DEM of the dashed box in Figure 1 with the locations of faulted outcrops. Each location is labeled along with major structures in western Guatemala.

2.1. Observations of Faulting in the Western Guatemala Wedge

Faulting is commonly observed within the western Guatemala wedge, even though both the Ellis et al. (2018, 2019) GPS velocity field and our updated velocity field indicate that there is little to no significant elongation occurring west of the Guatemala City graben (discussed more specifically within this article). This region also has a lack of historic seismicity with a single strike-slip earthquake focal mechanism recorded south of the western Motagua fault termination (Álvarez-Gómez et al., 2019; Authemayou et al., 2011). Due to the highly vegetated environment of western Guatemala and sparse outcrops, our approach was to characterize deformation in recently exposed road cuts (Figure 3). We have concentrated our efforts on four outcrops within the western Guatemala wedge. Three of the four outcrops are capped with unfaulted units and consequently indicate that deformation is inactive or occurs at very low strain rates at these sites. Additionally, these four outcrops form an east to west transect and fall into different geomorphic regions of western Guatemala.

Xenacoj, Location 1. The Xenacoj outcrop occurs west of the Mixco fault, the western boundary fault of the Guatemala City graben, and south of the Motagua fault. Within this region, steep valleys cut through thick volcanic deposits (Figure 3). In general, very little work has been published for this area. Ritchie (1975) mapped the San Juan Sacatepéquez quadrangle, which includes the Xenacoj outcrop, but only provided basic delineations of Neogene and Quaternary formations. Mapping of Quaternary units (mostly Pleistocene) suggest that these deposits originated from the Amatlán caldera to the southeast, as well as the widely distributed 75 ka Los Chocoyos ash from the Atitlán caldera to the west (Cisneros de León et al., 2021; Drexler et al., 1980; Koch & McLean, 1975; Rose et al., 1979, 1987, 1999; Wunderman & Rose, 1984; Figure 2).

Construction of a new highway near Santo Domingo Xenacoj, ~10 km west of the Mixco fault, exposed nearly 3 km of outcrop containing extensive faulting and numerous tephra and reworked deposits (Location 1, *Xenacoj*; Figures 3 and 4). One major fault, striking 124°, cuts nearly 40 m of outcrop and extends into the uppermost soil horizon. This major fault places a massive biotite-rich crystal vitric tuff (footwall block; sample 17JF65S in Table 1) adjacent to a younger series of faulted and unfaulted tephras, reworked sediments, and paleosols (hanging wall block). The biotite-rich crystal vitric tuff is heavily fractured, altered, and contains large blocks of biotite porphyry. Additionally, there is vertical variation in the igneous character of the deposit, more lava-like at the

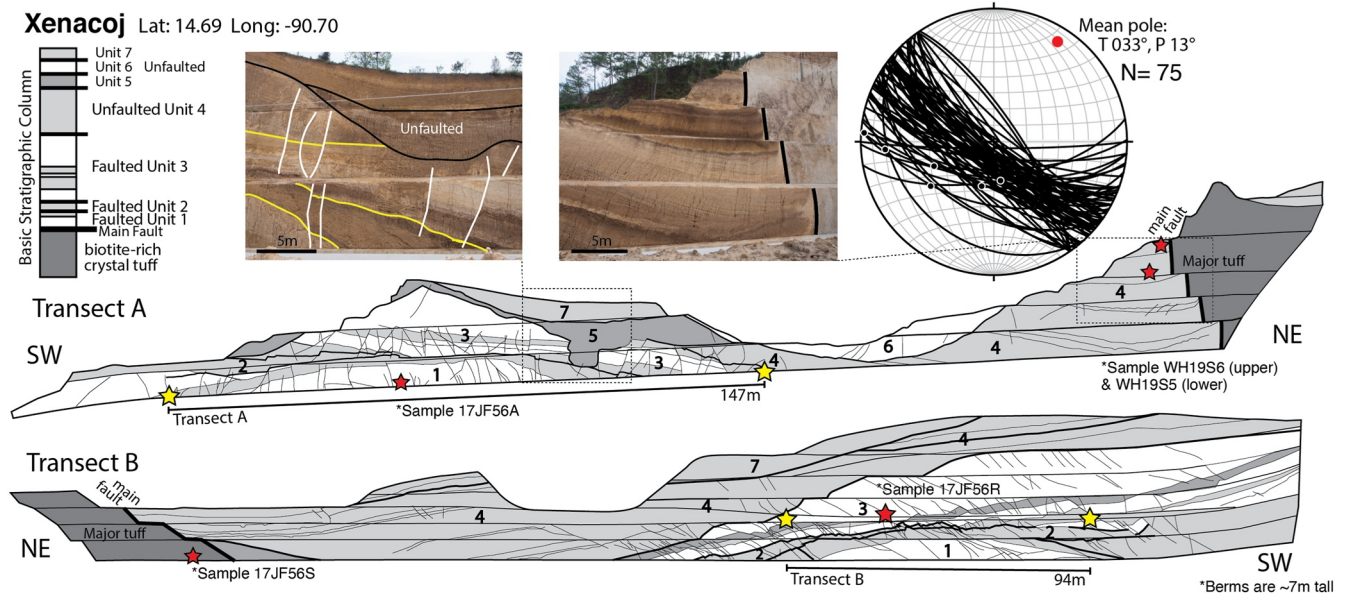


Figure 4. Annotated schematics of opposite facing roadcuts along the Santo Domingo Xenacoj highway (Location 1). Cross-section outcrop schematic shows the placement of the transects along the roadcut, original lengths, and orientation and length of the final transect imposed onto the orientation of maximum elongation. Stereonet displays the data from both transects. Stratigraphic units and faults are identified on the annotated outcrops. Unconformities are outlined with bolder lines, sections between unconformities are numbered 1 (oldest) to 7 (youngest) and correlated between outcrops. Yellow stars indicate transect endpoints and red stars show locations where samples were collected.

bottom and more pluton-like at the top, as well as less alteration at the bottom than top. While none of the deposits can easily be linked to the known stratigraphy by appearance, Ritchie (1975) and Williams (1960) briefly note a biotite-rich tuff that underlies much of this area. Offset markers and fault drag indicate normal-sense, down to the SW, movement of the main fault (Figure 4).

Faulting within the hanging wall was documented along two transects, which capture normal faulting that is capped by an erosional unconformity and a thick sequence of unfaulted volcanic and reworked deposits ($n = 75$, average trend = 300° ; Figure 4). The minor faults record tens of centimeters to meters of normal-sense offset. Slickenlines were only observed along six fault planes in Transect A (11% of fault planes), with four slickenlines with pitches ranging from 53° to 90° and two slickenlines pitching less than 25° . To constrain fault timing, three tephra deposits were sampled for $^{40}\text{Ar}/^{39}\text{Ar}$ dating and are described below (Table 1). Besides this outcrop, only sparse faulting was observed along other minor roadcuts or quarries within this region.

Tecpan, Location 2. The Chimaltenango basin extends between the Atilán Caldera and the Guatemala City graben, north of the volcanic arc (Figure 3). The basin is characterized as a flat plain with deep river valleys, often containing thick deposits of the Los Chocoyos tephra (75 ka) overlain by post-Los Chocoyos sediments (Clohan & Reynolds, 1977). Other tephra deposits from the Atilán and Amatitlán calderas, as well as other smaller sources, also cover this area (Figure 2).

A large roadcut south of the city of Tecpan exposes normal faults in a section of red volcanic sediments that are capped by thin and unfaulted, white tephra layers (Location 2 *Tecpan*, Figures 3 and 5). An irregularly shaped intrusion is also exposed on the SE end of the outcrop. Faults contain two orientations ($n = 14$ in total), a dominant orientation of $\sim 350^\circ$ ($n = 10$) and a secondary orientation of 055° ($n = 4$; Figure 5). Faults record tens of centimeters to meters of normal offset. No slickenlines were observed on fault planes. Mapping and descriptions by Clohan and Reynolds (1977) identify the red sediments as reworked deposits of the Los Chocoyos tephra (after 75 ka). The three white tephra layers that overlie faulted deposits were sampled for geochemistry and unit correlation analysis (samples WH19S7, WH19S8, WH19S9; Table 1).

Nahualá, Location 3. The area northwest of the Atilán caldera contains volcanic lavas and pyroclastic flows, tephra deposits, and structures related to the Atilán caldera, as well as other sources within the volcanic arc (Figure 3). The exact stratigraphy is difficult to distinguish due to numerous, small local Neogene and Quaternary

Table 1
Descriptions of Collected Samples

Sample	Location	Unit description	Mineralogy (including results from mineral count analysis)	Present structures	Age	Interpretation
WH19S5 (IGSN: IEBCGBG18)	Xenacoj outcrop, Lat: 14.695, Long: -90.696	Three thin felsic tephras (1.15, 1.17, and 1.3 m thicknesses) separated by paleosols. Each tephra contains pumice fragments and ash matrix		Unfaulted	56 ka (Cisneros de León et al., 2021)	Possibly I tephras from Amatitlan caldera
17JF56J (IGSN: IEBCGBG19)	Xenacoj outcrop, Lat: 14.695, Long: -90.696	White pumice-rich tephra containing pumice fragments, phenocrysts, and ash.	Pumice (up to 1.5 cm long) contains 4% mafic phenocrysts, 8% felsic phenocrysts, and 88% glass fragments. Mafic phenocrysts are biotite, hornblende, with 20% being magnetite.	Unfaulted	51 ka (Schindlbeck et al., 2016)	E tephra
17JF56R (IGSN: IEBCGBG16)	Xenacoj outcrop, Lat: 14.694, Long: -90.697	Thick, white, and gray tephra containing pumice fragments, phenocrysts, and ash. Pumice vesicles have the linear, spindle shape.	Pumice (1–3 cm long) contains up to 2% mafic phenocrysts, 3%–4% felsic phenocrysts, and 94%–97% glass fragments. Mafic phenocrysts are mostly biotite with a few grains of magnetite.	Faulted, NW-striking normal faults	1.145 ± 0.061 Ma (WiscAr lab, 2018)	
17JF56A (IGSN: IEBCGBG15)	Xenacoj outcrop, Lat: 14.694, Long: -90.698	Tan vitric tuff containing phenocrysts and glass fragments.	Tuff contains 14% mafic phenocrysts (dominantly biotite with lesser amounts of hornblende and magnetite), 30%–37% felsic phenocrysts, and 46%–53% glass fragments.	Faulted, NW-striking normal faults	1.495 ± 0.057 Ma (WiscAr lab, 2018)	

Table 1
Continued

Sample	Location	Unit description	Mineralogy (including results from mineral count analysis)	Present structures	Age	Interpretation
17JF56S (IGSN: IEBCGBG14)	Xenacoj outcrop, Lat: 14.694, Long: -90.696	Massive gray volcanic deposit, highly unsorted, containing large bombs of andesite porphyry, phenocrysts, and ash. Glass fragments are either light-gray colored with thin-walled, linear vesicles or dark gray colored with thick- walled, round vesicles.	Andesite porphyry blocks (Sample 17JF56S): Biotite, hornblende, and feldspar phenocrysts in a gray aphanitic matrix. Ash matrix (Sample 17JF56K) contains 2%–3% biotite phenocrysts, 8%–16% felsic phenocrysts, and 61%–68% glass fragments.	Faulted, NW-striking normal faults	9.117 ± 0.006 Ma (WiscAr lab, 2018)	Biotite-rich crystal vitric tuff
WH19S9 (IGSN: IEBCGBG11)	Tecpan outcrop; Lat: 14.716, Long: -90.957	Upper tephra containing angular pumice fragments, little sorted, reverse grading, and few lithics (1%–1.5%).		Unfaulted	56 ka (Cisneros de León et al., 2021)	Possibly I tephra from the Atitlan caldera
WH19S8 (IGSN: IEBCGBG10)	Tecpan outcrop; Lat: 14.716, Long: -90.957	Middle tephra of white and yellow pumice, well sorted, slight reverse gradation, 1%–2% fine lithics, and golden biotite (2%) and hornblende (1%) phenocrysts. Pumice fragments have very fine vesicles.		Unfaulted	51 ka	E tephra

Table 1
Continued

Sample	Location	Unit description	Mineralogy (including results from mineral count analysis)	Present structures	Age	Interpretation
WH19S7 (IGSN: IEBCGBG09)	Tecpan outcrop; Lat: 14.716, Long: −90.957	Lower tephra, ~1 m thick, contains pumice fragments and 5%–7% of basaltic lithics. Pumice fragments are light and gray in color and somewhat sorted. Horizons of irregular brown, oxidized layers up to 3 cm thick. Paleosol overlies tephra.		Unfaulted	54 ka	C tephra
14GM5b (IGSN: IEBCGBG20)	Tecpan outcrop; Lat: 14.717, Long: −90.959	Thick, red, reworked deposits of the Los Chocoyos. Rounded cobbles of various mafic lithologies, poorly sorted, in a clay-rich red/ tan matrix.		Faulted, N-S and NE-striking normal faults	Post-Los Chocoyos	Los Chocoyos sediments
14GM14M (IGSN: IEBCGBG12)	Nahuala outcrop; Lat: 14.821, Long: −91.347	Green-ish gray extrusive basalt/ andesite flow with foliation created by linear bands of light- colored minerals.	Aphanitic mafic matrix with thin, linear, parallel and anastomosing, olivine bands.	Unfaulted	3.227 ± 0.033 Ma (WiscAr lab, 2018)	Tertiary Cerro Jox basalt/andesite flow
14GM14k (IGSN: IEBCGBG13)	Nahuala outcrop; Lat: 14.820, Long: −91.348	2–3 thin white tephra layers, interlayered with soil horizons		Unfaulted	56 ka (Cisneros de León et al., 2021)	Likely I tephra from Atitlan caldera
Faulted Lithology (description only)	Nahuala outcrop; Lat: 14.821, Long: −91.347	Gray and white, indurated, lithic-rich lahar/mudflow deposit. Deposits contain rounded pebbles of andesite/basalt, broken felsic phenocrysts, in a gray, sandy matrix.		Faulted, NW-striking normal faults	Pliocene	Tertiary Lahars and mudflows

Table 1
Continued

Sample	Location	Unit description	Mineralogy (including results from mineral count analysis)	Present structures	Age	Interpretation
14GM7 (IGSN: IEBCGBG08)	Ilotenango outcrop; Lat: 15.041, Long: -91.228	>40 m thick, white, pumice-rich lapilli tephra. Very linear, spindle-shaped vesicles in pumice. Carbonized logs	Pumice (3–7 cm long) contains 96% glass, 4% felsic phenocrysts, and <1% mafic phenocrysts, nearly all of which are biotite.	Unfaulted	75 ± 2 ka (Cisneros de León et al., 2021)	Los Chocoyos tephra
14GM8 (lithologic description only)	Ilotenango outcrop; Lat: 15.041, Long: -91.227	Highly indurated tan reworked volcanic deposit with some visible layering and iron- stained bands. Possible lahar deposit based on unsorted and well indurated nature.		Faulted, NE-striking normal faults	Middle to Upper Miocene	Tertiary reworked deposit (Chalatenango or Balsamo Fm)

volcanic deposits. However, the area surrounding the Atitlán caldera is more thoroughly documented than any other area in western Guatemala, with basic unit descriptions reported (Clohan & Reynolds, 1977; Eggert & Lea, 1978; Holekamp et al., 1978; Hughes, 1978; Newhall, 1987; Rose et al., 1987; Williams, 1960).

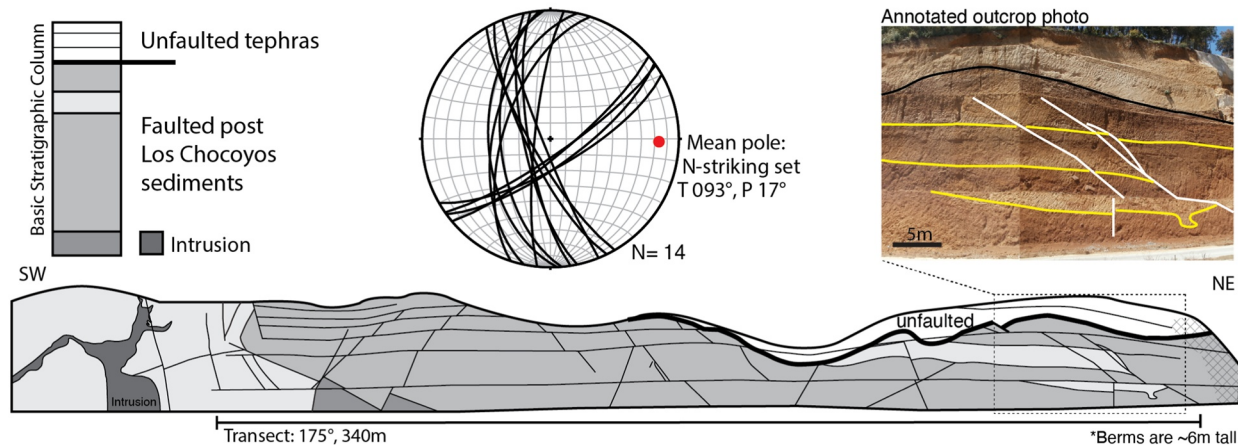
Faults are observed in a roadcut approximately 14 km northwest of Lake Atitlán, southwest of the city of Nahualá, in a highly indurated section of lahar flows and pebble/cobble conglomerates (Location 3, *Nahualá*; Figures 3 and 5). Fault strikes vary between 300° and 355° and normal-sense fault offsets ranging from centimeters to meters ($n = 14$). No slickenlines were observed on fault planes. A study by Eggert and Lea (1978) map the faulted units as Neogene reworked deposits and describe a few basalt flows in the area. An unfaulted, basalt/andesite flow caps the outcrop and the surrounding area (sample 14GM14, Table 1). Further, unfaulted, thin white tephra deposits overlie the flow.

Ilotenango, Location 4. The northwestern portion of the western Guatemala wedge is marked by linear, deep-cut river valleys that extend southeastward from the mountains just south of the Polochic fault (near Huehuetenango), to the tip of the Motagua fault, and southward to ~30 km behind the volcanic arc (Figures 1 and 3). River valley orientations change slightly across the area from ~045°—trending near Huehuetenango to ~032°—trending north of Lake Atitlán. The physical and geomorphic map of Guatemala (Alvarado Cabrera & Herrer Ibáñez, 2001) describes the river valleys as being fault controlled and related to movement on the Motagua fault. No other study analyzes the parallel river valleys of the region.

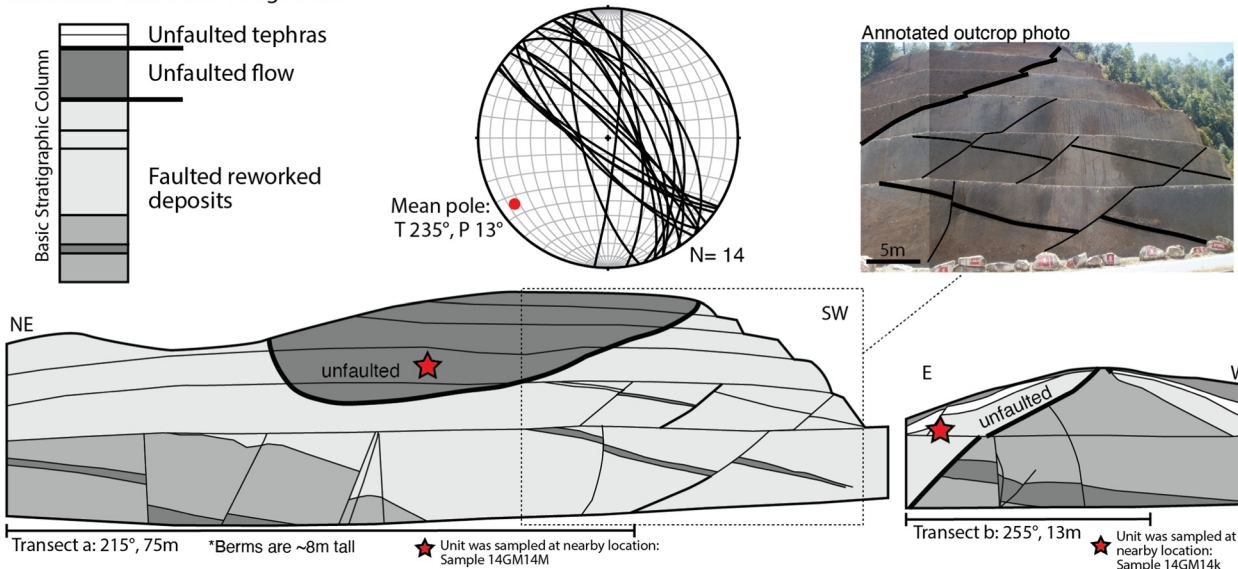
Williams (1960) describes that much of the river valley region is blanketed by a pink-topped tephra, which matches descriptions and mapping of the Los Chocoyos tephra by Rose et al. (1979, 1987, 1999) and Wunderman and Rose (1984). The Los Chocoyos tephra is underlain by Neogene tuffaceous sediments and conglomerates with dips as great as 30°. The Los Chocoyos ash is thickest in this region and can reach up to hundreds of meters in thickness in the deep valleys (Drexler et al., 1980; Rose et al., 1979, 1987, 1999; Wunderman & Rose, 1984). Other tephra from the Atitlán caldera also extend throughout the area (Figure 2).

Minor normal faulting is exposed on the eastern side of this region, in a small roadcut south of the town of San Antonio Ilotenango (Location 4, *Ilotenango*; Figures 3 and 5). Normal faults were recorded in a series of tan, fine-grained, indurated, reworked volcanic sediments, that are overlain by a thick, unfaulted white tephra (Figure 5). Fault orientations are nearly parallel to river valley orientations with strikes ranging from 020° to 030°, with tens of centimeters to meters of normal offset ($n = 25$). One slickenline was observed at this outcrop, with a

Tecpan Lat: 14.72 Long: -90.96



Nahuala Lat: 14.82 Long: -91.35



Ilotenango Lat: 15.04 Long: -91.23

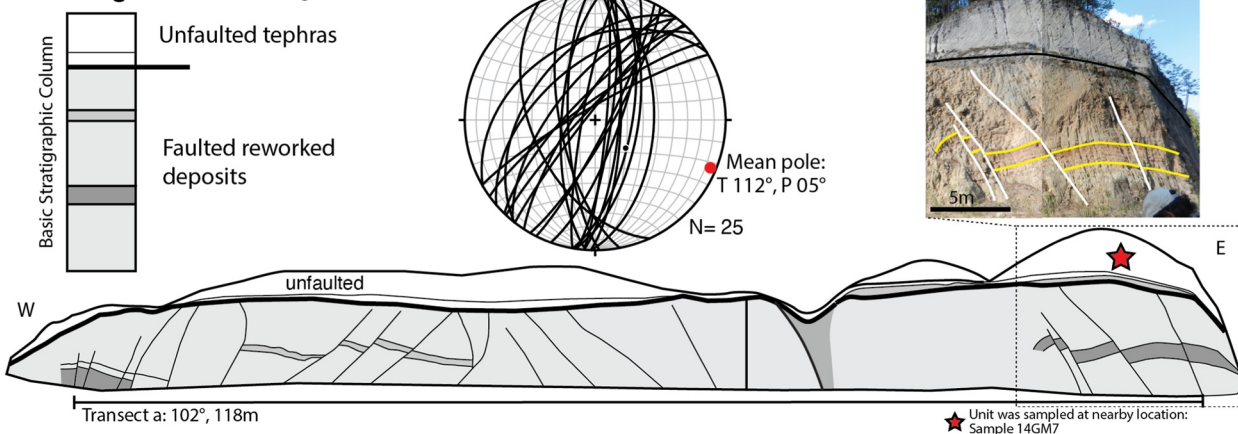


Figure 5. Annotated outcrops and data from locations 2, 3, and 4. Similar labels to those in Figure 4. In addition, an annotated outcrop photo is given for each location. There is no annotated outcrop for Ilotenango transect b (060°, 60 m).

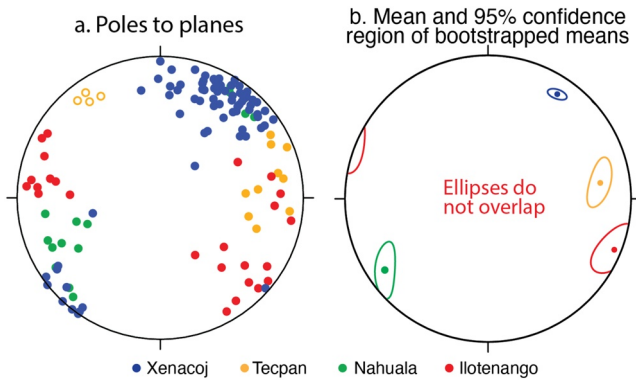


Figure 6. Fault data distribution, mean, and bootstrapped means. (a) Poles of all fault data are displayed on a left lower-hemisphere stereonet and color-coded by location. The open dots for Tecpan represent the secondary fault set that was removed for the elongation estimations and for the bootstrapped means. (b) The mean for each fault data set is projected, along with an ellipse that contains 95% of the bootstrapped mean. Ellipses for each data set do not overlap and indicate that the means are statistically different.

pitch of 77° . The overlying white tephra contains large white pumice blocks and charcoal logs and reaches a thickness of at least 100 m in nearby exposed quarries and valleys. These observations match descriptions and mapping of the 75 ka Los Chocoyos tephra and a sample was collected for geochemical analysis (sample 14GM7, Table 1).

2.2. Geodesy

The geodetic framework for this study and our related study of the nearby Jalpatagua fault (Garnier et al., 2020) is based on an updated elastic block model that assimilates new measurements at 32 GPS sites in northern Central America (locations are identified in Figure SA.1b in Supporting Information S1) into the regional model of Ellis et al. (2019), which was based on data as recent as early 2017. Of principal relevance for this study, new measurements from 17 campaign and continuous GPS sites in southern and western Guatemala extend the position time series at 10 campaign sites to at least 5 yr. Data are also included from three new campaign sites in western El Salvador (Garnier et al., 2020) and multiple new sites in central and western El Salvador (Legrand et al., 2020). Section 3.6 summarizes the methods that we use to estimate long-term velocities at these and other GPS sites in our study area.

3. Methods

3.1. Minor Fault Analysis

At each outcrop, fault observations (orientations, visible slickenlines, and fault separations on the outcrop face) were recorded along a transect of measured length, along with nearby bedding orientations. Each transect is bound on either end by a fault to avoid an unconstrained transect length, which can affect the calculated elongation (Titus et al., 2007). We observed very few slickenlines along fault surfaces at our outcrops: six slickenline measurements along Transect A at Xenacoj and no slickenlines observed along Transect B; no slickenlines were observed at Tecpan and Nahualá; and one slickenline measurement at Ilotenango. Marker beds indicate a normal sense of motion across nearly all fault planes and the majority of sparse slickenline data indicates downdip movement. Therefore, we assume normal, downdip movement for our collected fault data and this assumption was applied to the methods that follow. Samples were also taken for unit correlation purposes (e.g., the highest faulted unit and the lowest unfaulted unit, so fault timing could be constructed). Samples were not gathered from reworked deposits, which limits determining fault timing constraints at some outcrops. All gathered samples, fault data, and outcrops are briefly described in Table 1 and Figures 4 and 5.

3.2. Means and Statistical Tests

All collected normal fault data (poles to the plane) are displayed in Figure 6a to visualize the variation of fault orientations from the four outcrops. To explore the data sets with statistical methods, we applied methods explained in Davis and Titus (2017). Specifically, we determined a pole mean and 95% confidence ellipse of the bootstrapped pole means for each data set, using their code package for R (geologyGeometry: www.joshuadavis.us/software). For each location, the mean fault orientation was calculated by computing the eigenvector with the greatest eigenvalue from a scatter matrix of the pole data (*lineProjectedmean*). The secondary fault set for Tecpan (open circles in Figure 6a) was excluded from the Tecpan mean calculation and the following bootstrap application because the data differ enough from the main trend of fault orientations to skew the mean calculation and contains too few data to analyze on its own. The statistical method of bootstrapping was applied to each data set to compute 10,000 means from 10,000 synthetic data sets that were created by sampling with replacement (*lineBootstrapInference*). The synthetic data sets will have duplicates and omissions of the original data set and will generate slightly different means. This approach aims to simulate the variation of means from the larger fault population (all faults in the field). An elliptical confidence region was generated for each location that encompasses 95% of the bootstrapped means and serves as a method to compare the individual data sets. We observe

that no ellipses overlap among the four data sets (Figure 6), indicating that the means are statistically different for each area and fault populations are different.

3.3. Strain

One-dimensional strain, elongation, was calculated for each of the four outcrops containing normal faults observed in western Guatemala. The applied method focuses on calculating true displacement across faults, regardless of transect orientation (following methods outlined by Titus et al., 2007; Xu et al., 2007, 2009). The same approach was applied by Garibaldi et al. (2016) in the Salvadoran volcanic arc. A more thorough explanation can be found in Garnier et al. (2020) as applied to faulting in eastern Guatemala. In general, the direction of maximum elongation is determined by finding the orientation that maximizes the combined apparent heave of all faults along a transect, using the ratio between apparent heave and total heave (h_{app}/h_{total}). A graphical representation of this relationship for all outcrops is shown in Figure 7a.

For each transect, we calculated elongation based on measured faults (termed “elongation”), and then revised the calculation to include the collective offset of small, unobservable faults (termed “revised elongation”; Gross & Engelder, 1995; Marrett & Allmendinger, 1991, 1992; Walsh et al., 1991). Faults with orientations within 50° of the maximum elongation were used for each estimation. While each transect is bound by a fault on each end to constrain transect length, the offsets of these bounding faults are not included in the estimation (following Titus et al., 2007). In other words, the bounding faults are used to preserve fault spacing in order to measure a meaningful final transect length, but including the bounding fault offsets would overestimate the elongation. To calculate elongation from observed faults, the true horizontal heave was calculated for each fault and projected onto the maximum elongation direction. All horizontal heaves were combined to determine the collective heave in the direction of maximum elongation and the percentage of elongation (Table 2).

To include the effect of small faults, frequency-displacement plots (log of cumulative frequency vs. log of fault displacement, with 1 being the largest fault to n being the smallest fault) were generated to show the fractal quality of fault populations (Figure 7b). A slope was fitted to the linear portion of the frequency-displacement plot, representing intermediate faults that are often observed at outcrop level. The slope value (C) was used to compute the horizontal displacement due to small, unobservable faults (e.g., Gross & Engelder, 1995). The heave from small faults was added to the originally calculated heave and used to determine a revised percent elongation (Table 2, Figure 8).

Schematic diagrams of the original and resultant maximum elongation transects are shown in Figure 8. In general, there is a range of maximum elongation directions, varying from E-W to NNE-SSW, and elongation amounts, varying from 0.64% to 15.8%, determined from these minor fault arrays.

3.4. Unit Correlation

With elongation directions and amounts estimated from fault data, identifying faulted and unfaulted lithologies is needed to develop the deformational history of western Guatemala. Extensive studies on the major Guatemalan volcanic deposits have resulted in thorough unit descriptions, bulk pumice geochemistry data, tephra isopach maps, and geologic maps for individual deposit (Koch, 1970; Koch & McLean, 1975; McLean, 1970; Rose et al., 1981). These studies concluded that field evidence (unit appearance, thickness, location, and stratigraphic relationships to marker units) and pumice mineralogy (particularly the presence and amount of mafic phenocrysts) are the two best criteria for identifying and correlating Guatemalan units to the published data. For the Quaternary deposits, field evidence was used in combination with XRF data and pumice mineralogy from cleaned pumice fragments to link deposits to major tephra. For Neogene deposits, field evidence was the main method of unit correlation due to the lack of detailed data and analyses in the literature (Reynolds, 1977, 1980). Additionally, four samples were used for $^{40}\text{Ar}/^{39}\text{Ar}$ age analysis, to further correlate to the known stratigraphy and/or to determine the age of a previously undated unit. Data from these analyses are presented in Tables 1 and 3.

3.4.1. Pumice Geochemistry and Mineralogy

Major and trace element geochemistry of eight tephra samples was obtained by XRF analysis on washed pumice fragments (conducted by the Geoanalytical lab at Washington State University; data set in Geochem database: Garnier, 2021; Table 3). While most researchers conducting tephra correlation studies analyze glass geochemistry

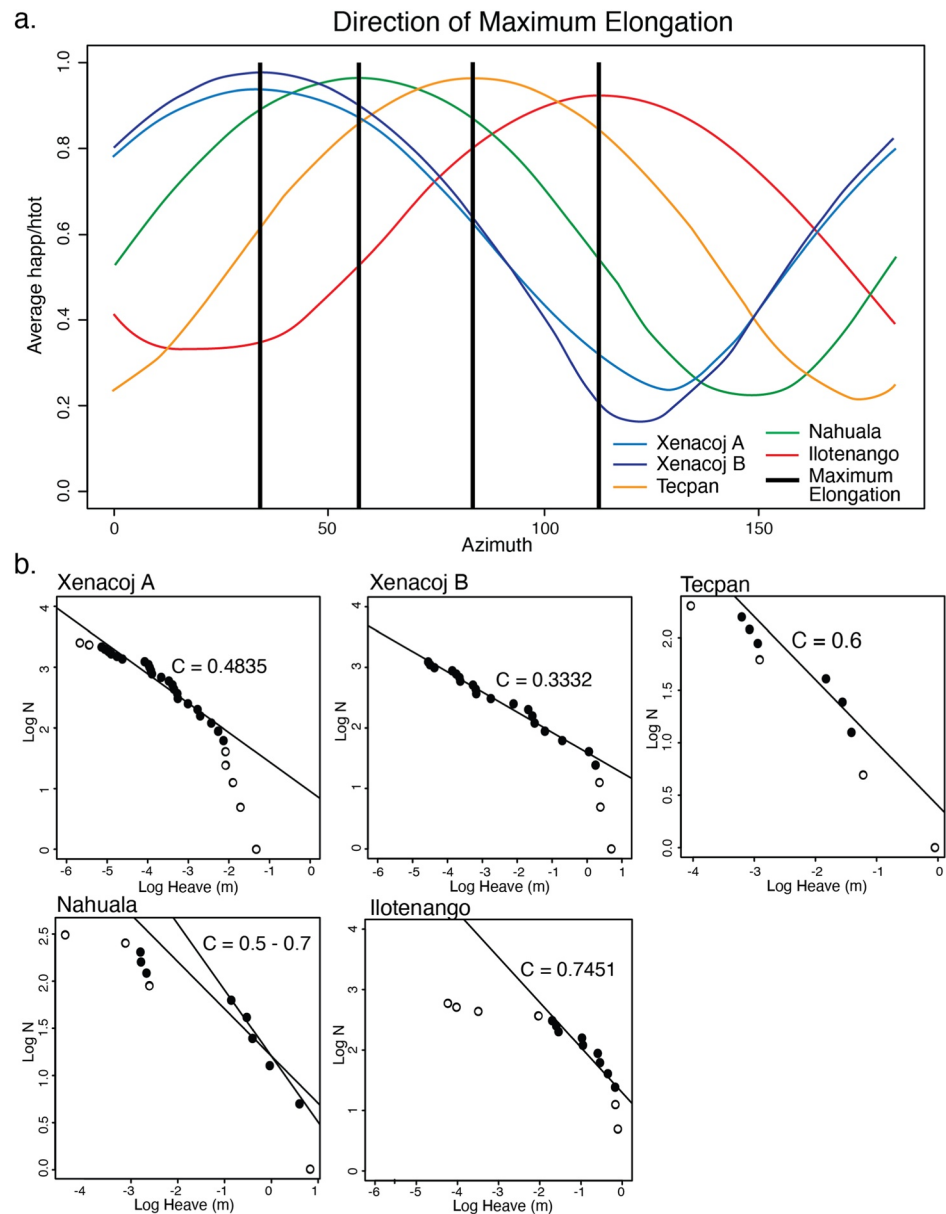


Figure 7. (a) Plot displaying the relationship between apparent heave (happ)/total heave (htot) and azimuth. The peak of each curve indicates the orientation of maximum elongation for each location. (b) Frequency-displacement plots for fault data at each outcrop. Black data points indicate those used in the regression.

by ICP-MS, the biggest drawback to this technique is low discrimination between tephra of the same or related sources, which is the situation in Guatemala with the two nearby rhyolitic sources of Atilán and Amatlán (Figure 2; Sarna-Wojcicki, 2000). Therefore, we compared the bulk pumice fragment geochemistry of our eight tephra samples, obtained by XRF analysis, to the documented geochemistry of the 10 major Quaternary tephra (Rose et al., 1987; Wunderman & Rose, 1984) by calculating similarity coefficients (Borchardt & Harward, 1971; Sarna-Wojcicki, 2000; Sarna-Wojcicki et al., 1984) between the two data sets. Similarity coefficients were calculated using the normalized weight percent of the following major elements: SiO₂, FeO, TiO₂, Al₂O₃, MgO, CaO, Na₂O, K₂O, and P₂O₅; and ppm of following trace elements: Sc, Ba, Rb, Sr, Zr, and La (Table 4). As geochemical analyses and reporting standards have changed over time, we were limited to only include the trace elements that were reported in common across all studies and data sets. Tephra pairs with the highest similarity coefficients were considered as potential correlations and compared to the field and dating evidence (Table 1).

Table 2
Minor Fault Analysis Results

Location	Lf (m)	Max elongation	# of Faults	dF (m)	Elongation (%)	he (m)	dFr (m)	Revised elongation (%)
West of Guatemala City graben								
<i>Xenacoj</i> 1a	86.8	33	44	1.49	1.7	0.123	1.76	2.1
<i>Xenacoj</i> 1b	78.5	34	23	8	11.3	0.086	8.1	11.5
<i>Tecpan</i> 2	212.6	83	10	0.83	0.4	0.52	1.34	0.64
<i>Nahuala</i> 3	166.4	56	13	6.3	3.9	0.42–1.1	6.7–7.4	4.2–4.7
<i>Ilotenango</i> 4	98.3	112	25	8.34	9.3	5.08	13.42	15.8

Note. Lf, Final length of transect; dF, Change in transect length due to faulting; he, Added length due to small, unobservable faults; dFr, Revised change in transect length due to observed and unobserved faults.

In addition to XRF analysis, pumice mineralogy was determined for five tephra samples. A mineral count analysis was conducted on crushed, clean pumice fragments, and results compared to previous work by Koch (1970), Koch and McLean (1975), and McLean (1970). Weight percentages of glass, felsic minerals, and mafic minerals, as well as mineral counts of the mafic phenocrysts, are included in Table 1 under Mineralogy.

3.4.2. $^{40}\text{Ar}/^{39}\text{Ar}$ Dating

$^{40}\text{Ar}/^{39}\text{Ar}$ dating was conducted on one tephra (pumice fragments from 17JF56R), one crystal-rich tuff (17JF56A), one andesite porphyry (17JF56S), and one basalt flow (14GM14M), all collected at faulted outcrops (Table 1). Plagioclase (250–500 μm) was isolated from the tephra, tuff, and porphyry samples. Groundmass (180–250 μm) was isolated from the basalt flow. The groundmass was treated with 1.2M HCl in an ultrasonic bath for 10 min, and then rinsed thoroughly with deionized water. Because some of the groundmass still showed evidence of alteration, additional ultrasonic leaching was done in a 3M HCl solution for 15 min followed by ultrasonic rinsing in deionized water and hand picking under a binocular microscope. The plagioclase was treated with 10% HF in an ultrasonic bath for 5 min, and then rinsed thoroughly with deionized water. The purified groundmass

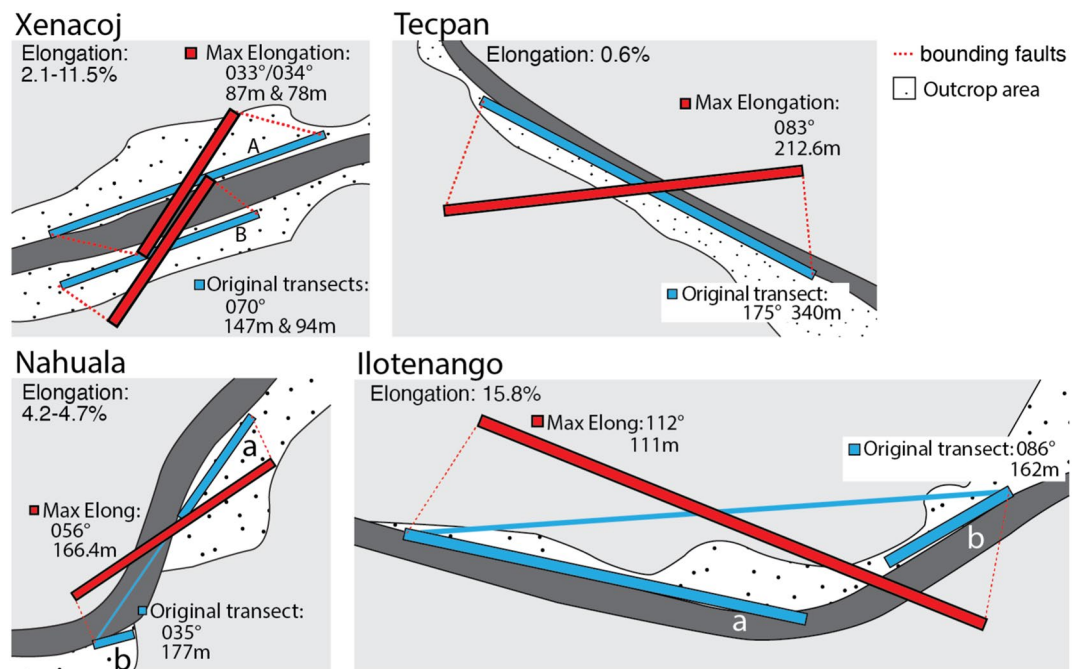


Figure 8. Map view schematics of each faulted outcrop. The length and orientation of the original faulted transects are displayed in blue and the transect projected onto the maximum elongation orientation are displayed in red. Red dashed lines are the orientation of the bounding faults.

Table 3
XRF Data From Collected Samples Within the Western Guatemala Wedge

Sample Id	17JF56S	17JF56A	17JF56R	17JF56J	WH19S5	WH19S7	WH19S8	WH19S9	14GM14k	14GM7
IGSN	IEBCGBG14	IEBCGBG15	IEBCGBG16	IEBCGBG19	IEBCGBG18	IEBCGBG09	IEBCGBG10	IEBCGBG11	IEBCGBG13	IEBCGBG08
Location	Xenacoj	Xenacoj	Xenacoj	Xenacoj	Xenacoj	Tecpan	Tecpan	Tecpan	Nahuala	Ilotenango
Latitude	14.694	14.694	14.694	14.695	14.695	14.716	14.716	14.716	14.82	15.041
Longitude	-90.696	-90.698	-90.697	-90.696	-90.696	-90.957	-90.957	-90.957	-91.348	-91.228
Normalized major elements (Weight %):										
SiO ₂	74.43	69.72	74.27	70.72	68.56	68.1	72.89	76.01	67.35	77.37
TiO ₂	0.345	0.37	0.236	0.435	0.411	0.422	0.349	0.136	0.454	0.11
Al ₂ O ₃	14.31	17.37	16.49	16.73	19.45	17.62	14.72	14.28	18.18	12.97
FeO*	1.8	3.06	1.7	2.37	3.42	3.97	2.2	0.86	3.42	0.66
MnO	0.035	0.067	0.062	0.101	0.14	0.135	0.091	0.073	0.106	0.067
MgO	0.32	0.75	0.2	0.54	0.71	1.1	0.55	0.17	0.84	0.12
CaO	0.61	2.35	0.85	1.45	2.32	3.04	1.42	0.82	3.2	0.81
Na ₂ O	3.23	3.22	2.39	3.77	3.11	3.65	3.65	3.36	3.68	3.64
K ₂ O	4.92	3.08	3.78	3.83	1.81	1.89	4.11	4.27	2.66	4.24
P ₂ O ₅	0.005	0.016	0.02	0.067	0.063	0.077	0.023	0.021	0.117	0.014
Total	100	100	100	100	100	100	100	100	100	100
Trace elements (ppm):										
Ni	6	5	4	4	3	3	3	3	5	3
Cr	3	3	3	3	2	3	3	5	3	2
Sc	3	8	4	5	6	6	4	3	8	2
V	16	45	18	19	28	52	24	7	52	2
Ba	810	885	988	1,149	1,016	861	1,045	1,019	892	1,012
Rb	217	89	98	102	42	48	117	118	92	122
Sr	76	260	97	193	306	351	152	115	378	102
Zr	236	130	104	289	189	142	247	66	190	61
Y	23	19	17	27	20	14	20	11	17	11
Nb	14.4	5.5	6.9	7.6	4.2	3.3	6.5	5.6	6.6	6
Ga	17	16	14	17	18	17	14	13	19	13
Cu	1	9	7	7	9	17	6	6	10	2
Zn	49	44	31	54	69	66	47	25	75	24
Pb	20	13	14	16	12	9	15	14	22	14
La	37	28	22	25	20	12	19	19	24	20

Table 3
Continued

Sample Id	17JF56S	17JF56A	17JF56R	17JF56J	WH19S5	WH19S7	WH19S8	WH19S9	14GM14K	14GM7
Ce	52	39	38	48	36	24	41	35	39	34
Th	15	9	10	8	4	3	8	12	8	12
Nd	24	20	17	24	18	14	14	12	17	13
U	5	3	4	3	2	1	4	4	2	3

Note. Data accessible in Geochem database (Garnier, 2021).

and plagioclase separates were wrapped in an aluminum foil packet and irradiated with 1.1864 Ma Alder Creek sanidine. At the University of Wisconsin-Madison WiscAr Laboratory, ~15 mg of groundmass from the basalt sample was incrementally heated using a 50W CO₂ laser and single crystal total fusion experiments were performed on the plagioclase from the tephra, tuff, and porphyry samples. All analyses were done using a Noblesse 5-collector mass spectrometer following the procedures in Jicha et al. (2016). Results are summarized in Tables 5 and 6 and Figure 9 (complete data is available in Table SB.1 in Supporting Information S1).

3.5. Elongation Rate

We calculated elongation rates for each of the four outcrops using: (a) the estimated elongation; and (b) ages of faulted and unfaulted deposits which delimit the timing of deformation. To determine elongation rate, the amount of added length for each outcrop (dFr in millimeters, Table 2) was divided by the estimated time span of active faulting (age of youngest faulted unit minus overlying, unfaulted deposit, in years; Table 7). Elongation rates were similarly calculated in the El Salvador fault zone by Garibaldi et al. (2016). Since we can only determine the end points of the period of active faulting, all elongation rates are minimums (all data displayed in Table 7).

3.6. GPS Velocity Field

We used the new GPS data described in Section 2.2 to update the Ellis et al. (2019) regional block model in three stages. We first processed the raw GPS data via methods described by Ellis et al. (2018). We then inverted the up-to-date GPS position time series for all 215 stations included in our analysis, including all ~200 stations that were used by Ellis et al. (2018), to estimate an updated time-dependent regional elastic model that corrects all the GPS position time series for the effects of three earthquakes that disrupted our study region during the period spanned by our GPS measurements, namely the May 28, 2009 $M_w = 7.3$ Swan Islands earthquake, the August 27, 2012 $M_w = 7.3$ El Salvador earthquake, and the November 07, 2012 $M_w = 7.4$ Champerico earthquake. The GPS station velocities from this inversion, which are corrected for the coseismic and postseismic effects of all three earthquakes, are found in Table SA.1 in Supporting Information S1 (Columns 13 and 14). The time-dependent modeling methods and assumptions are described in detail by Ellis et al. (2018).

A comparison of our newly estimated velocities to the Ellis et al. (2019) velocity field (Figure SA.1a in Supporting Information S1) reveals differences of only a few tenths of a mm/yr or less at most locations (Figure SA.1b in Supporting Information S1). The largest velocity differences, which range from 1 to 4 mm/yr, occur mostly at the campaign sites in our study area (western and southern Guatemala), where our new observations significantly lengthen the previously short time span of the observations at those sites.

The final stage of our geodetic analysis consists of an inversion of all 215 GPS site velocities from the updated time-dependent solution described above to estimate a new regional elastic block model. The methods and block model parameterization that we used for our inversion are identical to those described by Ellis et al. (2019). Both the previous and updated models incorporate eight plates and/or blocks (e.g., Figure SA.2b in Supporting Information S1), of which angular velocities are estimated for the Chortis, Ipala, Fonseca, and Motagua-Polochic blocks and the CAFA. Similar to results reported by Ellis et al. (2019; see their Section 4.1), our updated GPS velocity field is consistent with the existence of independent, internally deforming Chortis and Ipala blocks (blocks with green and purple arrows, respectively, in Figure 10). The other estimated parameters include the magnitudes and distributions of interseismic locking for the Middle America subduction zone, the Motagua-Polochic fault, and strike-slip faults along the Central America volcanic arc. Strain-rate tensors are also estimated for the Ipala, Chortis, and Fonseca blocks. During the inversion, the angular velocities for the Caribbean, Cocos, and North America plates are fixed to values that were estimated in advance from well-determined GPS site velocities from those plates and the MORVEL plate motion model (blue and black arrows in Figure 11; DeMets et al., 2010).

The results from the inversion are presented below (Section 4.5). Other inversion outputs of interest for our study are the GPS site velocities that are corrected for the elastic effects of all the active faults in the block model, which approximate the long-term plate/block motions and distributed deformation that we require for this study. The velocities displayed in Figure 10 are given in the Caribbean plate frame of reference. In contrast, the velocities displayed in Figures 11 and 12 and tabulated in Table SA.1 in Supporting Information S1 (Columns 12 and 13) are given in the North America plate frame of reference defined in Table 1 of Ellis et al. (2019) and also indicated in the footnotes to Table SA.1 in Supporting Information S1.

Table 4
XRF Similarity Coefficient Between Collected Samples and Quaternary Tephtras

	14GM7	14GM14k	WH19S7	WH19S8	WH19S9	17JF56J	WH19S5
I falls	0.57	0.82*	0.77	0.8	0.62	0.81	0.85*
E	0.58	0.75	0.69	0.85*	0.62	0.91*	0.76
C	0.49	0.90*	0.84*	0.66	0.52	0.73	0.81*
H flow low K average	0.63	0.71	0.69	0.75	0.66	0.76	0.74
H flow high K average	0.91*	0.5	0.47	0.71	0.92	0.61	0.51
H fall average	0.87*	0.54	0.51	0.73	0.89	0.64	0.54
Tflow	0.61	0.7	0.64	0.86	0.66	0.9	0.71
Tt fall	0.62	0.7	0.64	0.87	0.67	0.9	0.71
Z5	0.57	0.73	0.67	0.82	0.61	0.93	0.75
Z4	0.56	0.76	0.7	0.82	0.6	0.91	0.76
Z2	0.47	0.82	0.86	0.63	0.49	0.68	0.81
W flow average	0.67	0.65	0.62	0.8	0.72	0.76	0.64
W fall average	0.64	0.71	0.68	0.78	0.67	0.78	0.73
Lf(2)	0.56	0.73	0.67	0.8	0.6	0.89	0.73
Lf(1)	0.53	0.76	0.69	0.73	0.56	0.84	0.74
Lt	0.59	0.71	0.64	0.84	0.63	0.91	0.71

Note. **bold*** coefficients are the highest values for a given sample.

4. Results

4.1. Xenacoj, Location 1

Results from the minor fault analysis and $^{40}\text{Ar}/^{39}\text{Ar}$ dating of three samples from the Xenacoj outcrop, west of the Guatemala City graben, indicate that large volcanic and faulting events occurred in this area during the Neogene and Quaternary. The height of the faulted outcrop indicates that the main fault (striking 124°) accommodated at least 40 m of normal movement to the southwest. Folding of the hanging wall deposits also suggests that the main fault may have a listric shape in the subsurface, while thickening of individual layers toward the main fault suggests periods of syndepositional faulting.

From minor faults measured along two transects, we estimate that 2.1% and 11.5% of $033^\circ/034^\circ$ -directed elongation occurred within the hanging wall block (Figure 8). The difference in estimated elongations is most likely attributed to one large area of distributed strain in Transect A, where it was difficult to determine precise fault planes and offsets. Transect B only contained clear fault planes and offsets. Therefore, we suggest that the estimated 11.5% elongation from transect B, although in younger sediments, is more representative of the elongation that occurred prior to the overlying unconformity. Additionally, faulting from both transects appear to represent the same deformational events (Figure 4).

Observed deposits do not correlate to any of the known tephtras in the literature, yet the large volume/thickness of volcanic deposits and bolder-sized blocks within the biotite tuff suggest that large eruptive events have occurred from unknown, nearby source(s). Previous studies have also documented these large pre-Quaternary deposits,

Table 5
Summary of $^{40}\text{Ar}/^{39}\text{Ar}$ Total Fusion Analyses

Sample #	Location	Wt. % SiO ₂	Latitude (N)	Longitude (W)	Material	N	MSWD	Weighted mean age (Ma) $\pm 2\sigma$
17JF56R	Xenacoj	74.3	14.6943	90.6968	Plagioclase	6 of 8	1.2	1.145 \pm 0.061
17JF56A	Xenacoj	69.7	14.6943	90.6968	Plagioclase	3 of 7	0.05	1.495 \pm 0.057
17JF56S	Xenacoj	74.4	14.6948	90.6962	Plagioclase	16 of 17	1.4	9.115 \pm 0.008

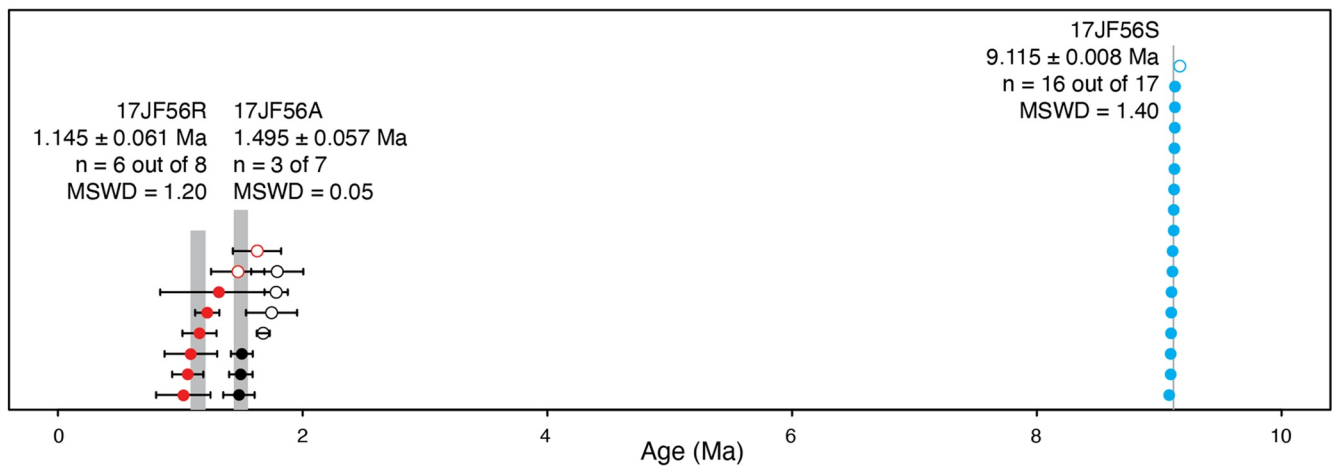
Table 6
Summary of $^{40}\text{Ar}/^{39}\text{Ar}$ Incremental Heating Analyses

Sample #	Location	Wt. % SiO_2	Latitude (N)	Longitude (W)	Material	$^{40}\text{Ar}/^{36}\text{Ar}_i \pm 2\sigma$	Isochron age (Ma) $\pm 2\sigma$	N	^{39}Ar %	MSWD	Mean age (Ma) $\pm 2\sigma$
14GM14	Nahuala	67.4	14.8215	91.3472	Groundmass	289.3 ± 9.8	3.227 ± 0.033	14/31	44	1.07	3.2 ± 0.009

Note. All ages in Tables 5 and 6 are calculated relative to the Alder Creek sanidine standard at 1.1864 Ma (Jicha et al., 2016) using decay constants of Min et al. (2000).

but have not been able to accurately map and define the units or determine the source (Ritchie, 1975; Williams, 1960). $^{40}\text{Ar}/^{39}\text{Ar}$ dating of the three samples gave weighted mean ages of 9.115 ± 0.008 Ma (Late Miocene) for the massive biotite-rich crystal vitric tuff in the footwall (17JF56S), 1.495 ± 0.057 Ma (Pleistocene) for the lowest, faulted tan vitric tuff in the hanging wall (17JF56 A, Unit 1), and 1.145 ± 0.061 Ma (Pleistocene) for the highest, faulted gray pumice lapilli tuff in the hanging wall (17JF56 MR, Unit 4; Figure 9a; Table 5). Additionally,

a. Xenacoj



b. Nahuala

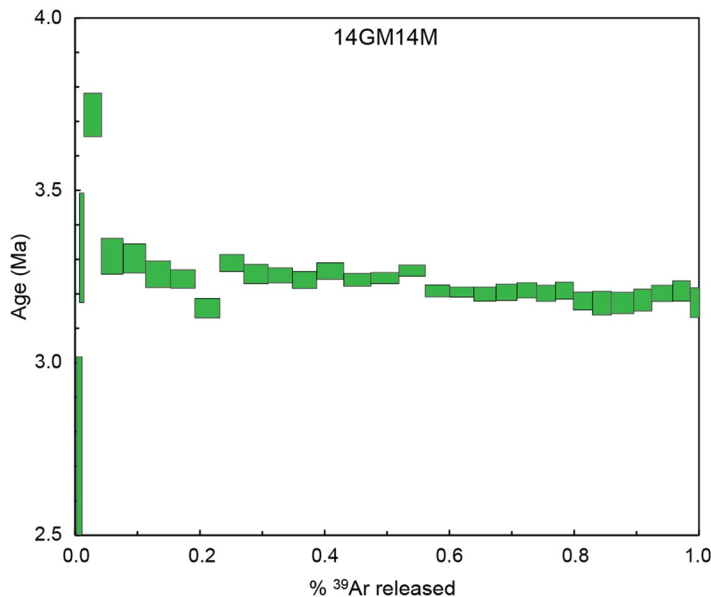


Figure 9. $^{40}\text{Ar}/^{39}\text{Ar}$ data for four samples collected in western Guatemala. (a) Rank order plots for the three tephra samples collected at Location 4 (17JF56R, 17JF56A, and 17JF56S). White dots are not included in weighted mean calculations. (b) Age spectrum diagram for sample 14GM14M (Nahualá). The data do not yield a plateau. However, because most of the heating steps give ages between 3.3 and 3.2 Ma, we tentatively assume that this is a fair approximation for the age of this sample.

Table 7
Estimated Elongation Rates for Faulted Outcrops

Outcrop	Length added (dFr from Table 2, mm)	Upper limit of fault timing (age of unfaulted deposit)		Lower limit of fault timing (age of youngest faulted deposit)		Time span	Strain rate (mm yr ⁻¹)
		Deposit	Age	Deposit	Age		
Xenacoj 1a	1,760	E tephra, youngest unfaulted deposit	51 ka	Faulted gray tuff, sample 17JF56R	1.145 ± 0.061 Ma	1.1 Ma	0.0016
Xenacoj 1b	8,100						0.007
Tecpan	1,340	C tephra	54 Ka	Los Chocoyos	75 ± 2 ka	21 ka	0.063
Nahuala	6,700–7,400	Cerro Jox basalt/andesite flow	3.2 Ma	Balsamo formation (Late Miocene boundary)	11.14 Ma	7.94 Ma	0.0008–0.0009
Ilotenango	13,420	Los Chocoyos	75 ± 2 ka	Balsamo or Chalatenango formations	2.58 Ma or 5.33 Ma	2.51–5.26 Ma	0.003–0.005
Ilotenango (extrapolated area)	6,320,000	Los Chocoyos	75 ± 2 ka	Balsamo or Chalatenango formations	2.58 Ma or 5.33 Ma	2.51–5.26 Ma	1.2–2.5

plagioclase from one tephra (17JF56J) sampled near the surface (Unit 4) lacked radiogenic Ar. However, this sample appears geochemically similar to the E tephra from the Amatitlán caldera. The age of the E tephra from Amatitlán is estimated at 51 ka, based on sedimentation rates in ocean cores (Schindlbeck et al., 2016).

By combining the structural and stratigraphic data, faulting in Transects A and B occurred in the Pleistocene, after deposition of 1.145 ± 0.061 Ma gray tuff and before deposition of the thick unfaulted sequence of tephtras and sediments. Since we are unable to date the stratigraphically lowest members of the unfaulted sequence, fault timing cannot be constrained beyond using the youngest unfaulted 51 ka white tephra deposited near the surface, which would provide a window of ~1.1 Ma for the Transect B recording 11.5% elongation, which indicates a minimum elongation rate of 0.007 mm/yr for the outcrop (Figure 13; Table 7). A more detailed deformational and stratigraphic history of this outcrop is outlined in Text SC.1 in Supporting Information S1 and Figure SC.1 in Supporting Information S1.

4.2. Tecpan, Location 2

Minor faulting at the Tecpan outcrop suggests 0.64% of elongation occurred at a direction of 083°, based on the dominant ~N-NNW-trending normal fault set (Figure 8). A primary N-NNW fault set and secondary NE-trending faults parallel other lineaments identified by Clohan and Reynolds (1977) within this area. As previously stated, faulting occurred in post-Los Chocoyos reworked deposits (after 75 ka). Similarity coefficients suggest that the overlying, unfaulted tephtras are geochemically similar to multiple Pleistocene tephtras. However, by eliminating tephtras older than the Los Chocoyos, we suggest that the lower two tephtras best represent the C and E tephtras from the Amatitlán caldera (ages of 54 and 51 ka, respectively; Schindlbeck et al., 2016, see Figure 2). The uppermost tephra could not be correlated to a post-Los Chocoyos tephra based on the available data. Therefore, faulting in this area most likely occurred in a short period during the Pleistocene, between deposition of the Los Chocoyos and C tephtras (75 and 54 ka, a 21 ka span; Figure 13). If the timing estimate is correct, it indicates a low elongation rate of 0.063 mm/yr of 083°—elongation at the faulted outcrop (Table 7).

4.3. Nahualá, Location 3

From minor faulting within the Nahualá outcrop, we estimate 4.2%–4.7% elongation occurred in a maximum elongation direction of 056° (Figure 8). The dominant presence of andesitic material in the faulted, reworked lahar and conglomerate deposits suggest that they belong to the Bálsamo formation, extending from Late Miocene through the Pliocene. This interpretation agrees with mapped Neogene lahar deposits by Eggert and Lea (1978). The overlying basalt flow did not yield a plateau, but most of the heating steps give ages between 3.3 and 3.2 Ma (Figure 9b; Table 6), which we use as an approximation for its age. This sample closely matches descriptions of the Tertiary Cerro Jox Andesite flow of Eggert and Lea (1978). Thin white, unfaulted tephtras overlie the flow and are most similar geochemically to the I tephra fall deposits (56 ka) from Atitlán (Cisneros de León et al., 2021;

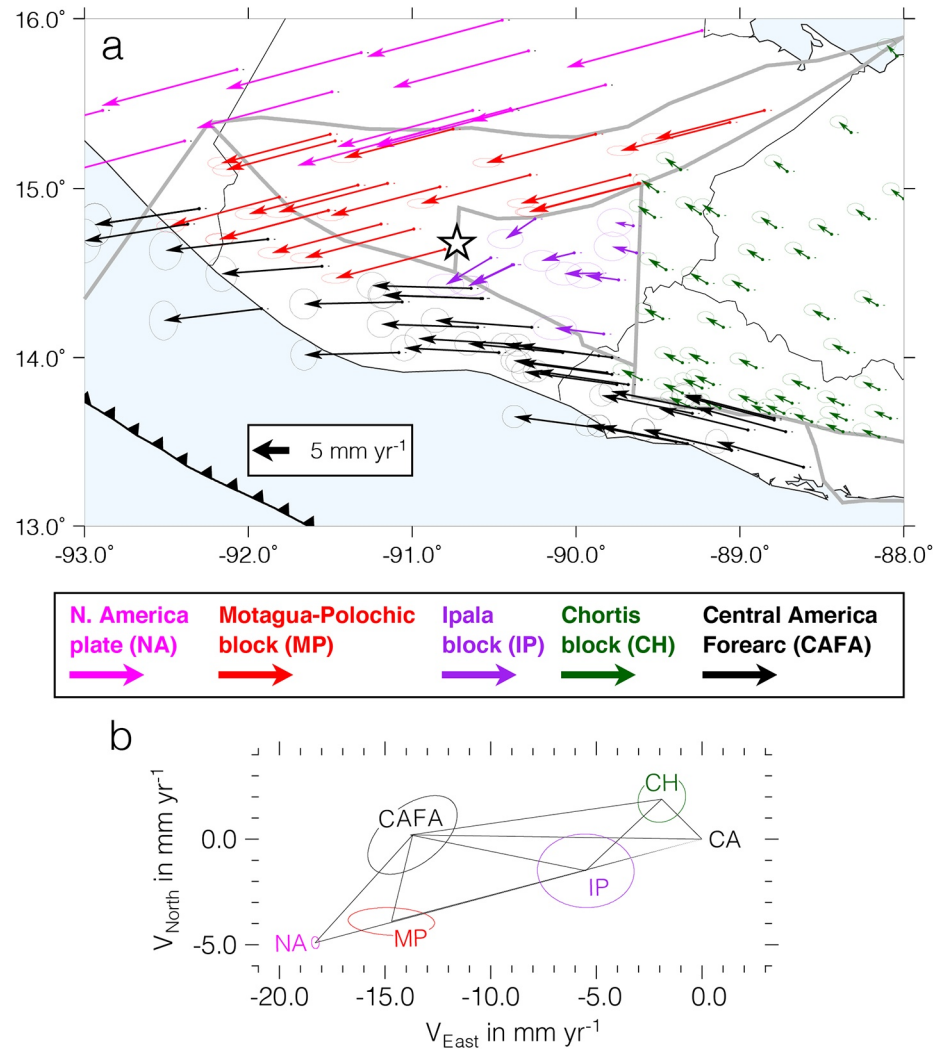


Figure 10. (a) Long-term velocity components at each GPS site estimated from the TDEFNODE elastic block model described in the text. The long-term velocity component at each site is estimated from the angular velocities in Table SA.2 in Supporting Information S1 and any estimated internal distributed deformation for each block, but excludes interseismic elastic motion due to locked faults in the model. All velocities are relative to the Caribbean (CA) plate. The open star near the center of the map denotes the location where the velocities in Panel (b) were calculated. The bold gray lines define the elastic block boundaries. (b) Plate and block linear velocities at the Guatemala City graben as determined from the angular velocities in Table SA.2 in Supporting Information S1. The plate and block abbreviations and colors are defined in the legend. The ellipses show the 2-D, 1-sigma uncertainties. “CA” in the velocity diagram represents the Caribbean plate.

Rose et al., 1999) and fall within the mapped depositional area of this tephra. Therefore, NE-elongation at the Nahualá outcrop likely took place in the Miocene, after deposition of the Middle Miocene reworked unit, and ceased before deposition of the ~3.2 Ma flow, with no obvious faulting of Pleistocene and earlier deposits in the area (Figure 13). If we use the Late Miocene boundary for the Bálsamo formation (11.14 Ma) and the range of elongation amounts, it indicates an elongation rate of almost 0.001 mm/yr (Table 7). This estimate is very conservative without a more precise age for the faulted deposits.

4.4. Ilotenango, Location 4

Results from the minor fault analysis at the Ilotenango outcrop indicate that 15.8% elongation has occurred in a maximum elongation direction of 112°, which is roughly perpendicular to the orientation of nearby river valleys (Figure 8). Field evidence, geochemistry, and pumice mineralogy indicate that the overlying, unfaulted white tephra correlates to the Los Chocoyos ash (75 ka). Faulted deposits are most likely Neogene in age, based on

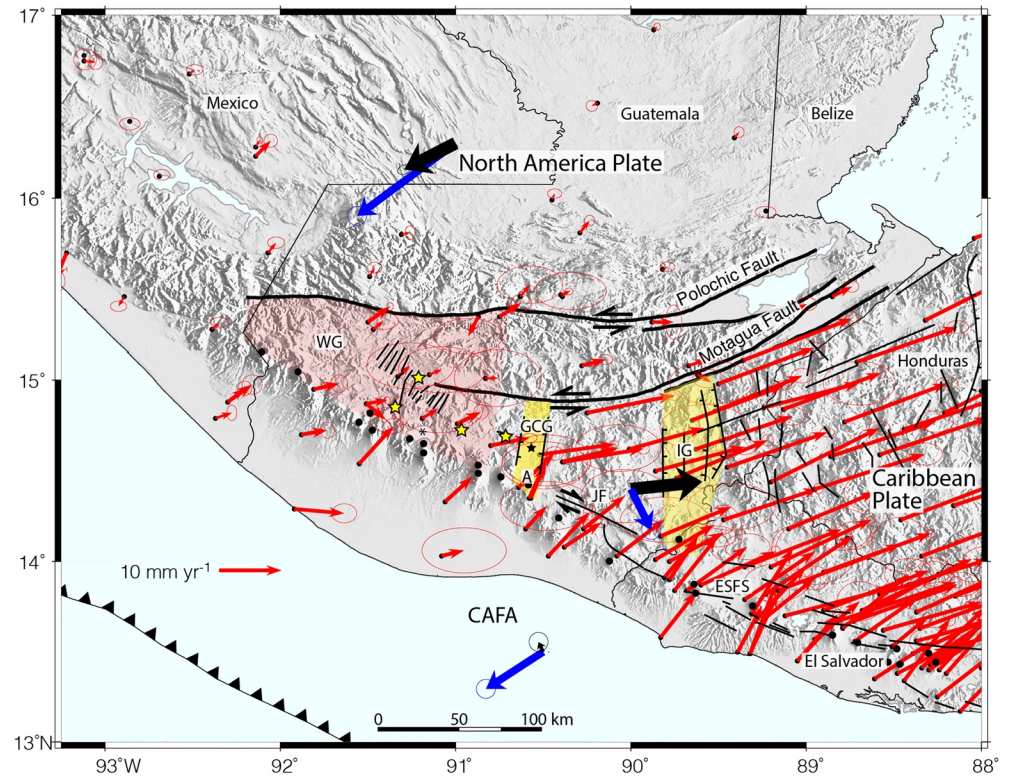


Figure 11. Observed GPS site velocities relative to a stationary North America plate (red arrows), corrected for elastic deformation attributed to locked faults in the study area. The velocities in the figure are found in Table SA.1 in Supporting Information S1. Bold black and blue arrows show absolute velocities of the North America and Caribbean plates and Central American Forearc in mantle-fixed (Wang et al., 2018) and no-net-rotation (Argus et al., 2011) frames of reference. Ellipses show the 1-sigma uncertainties. Red shaded region defines the western Guatemala wedge, while the large Guatemala City and Ipala grabens are shaded yellow. Abbreviated features: WG, Western Guatemala wedge; GCG, Guatemala City graben (black star- Guatemala City); A, Amatitlán caldera; JF, Jalpatagua fault; IG, Ipala graben; ESFS, El Salvador fault system; CAFA, Central American Forearc. Yellow stars represent faulted outcrops used in minor fault analysis, larger black dots mark volcanoes.

descriptions by Williams (1960), but a more precise age could not be determined due to the reworked nature of the deposits and the lack of individually defined Neogene deposits in the literature. If the Neogene deposits are assigned to the Bálamo formation (Upper Miocene to Pliocene) or the Chalatenango formation (Middle/Upper Miocene), faulting would have occurred after 2.58 or 5.33 Ma, respectively, and ceased by 75 ka (Figure 13). A time span of 2.51–5.26 Ma would indicate a slow elongation rate of 0.003–0.005 mm/yr for the transect. If the elongation results from Ilotenango are applied to the entire region of linear river valleys (15.8% elongation over ~40 km at an orientation of 112°), 6.32 km of added length would indicate a minimum extension rate of 1.2–2.5 mm/yr for the region (Table 7).

4.5. Updated Geodetic Elastic Block Model

Our new elastic block model results closely resembles those of Ellis et al. (2019), as expected given the large overlap in their underlying data and their identical model parameterizations. Due mostly to larger misfits for several new GPS site velocities from the Fonseca block, the newly estimated model has a weighted root-mean-square (WRMS) misfit of 1.16 mm/yr, modestly larger than the 1.03 mm/yr WRMS misfit for the previous model. The newly estimated angular velocities, which are given in Table SA.2 in Supporting Information S1, predict block motions that are close to those estimated with the angular velocities determined by Ellis et al. (2019). At most locations, the fault slip rates estimated with the plate/block angular velocities differ by less than 0.5 mm/yr for the two models (Figure SA.2 in Supporting Information S1), less than the ± 1 mm/yr or larger fault slip rate

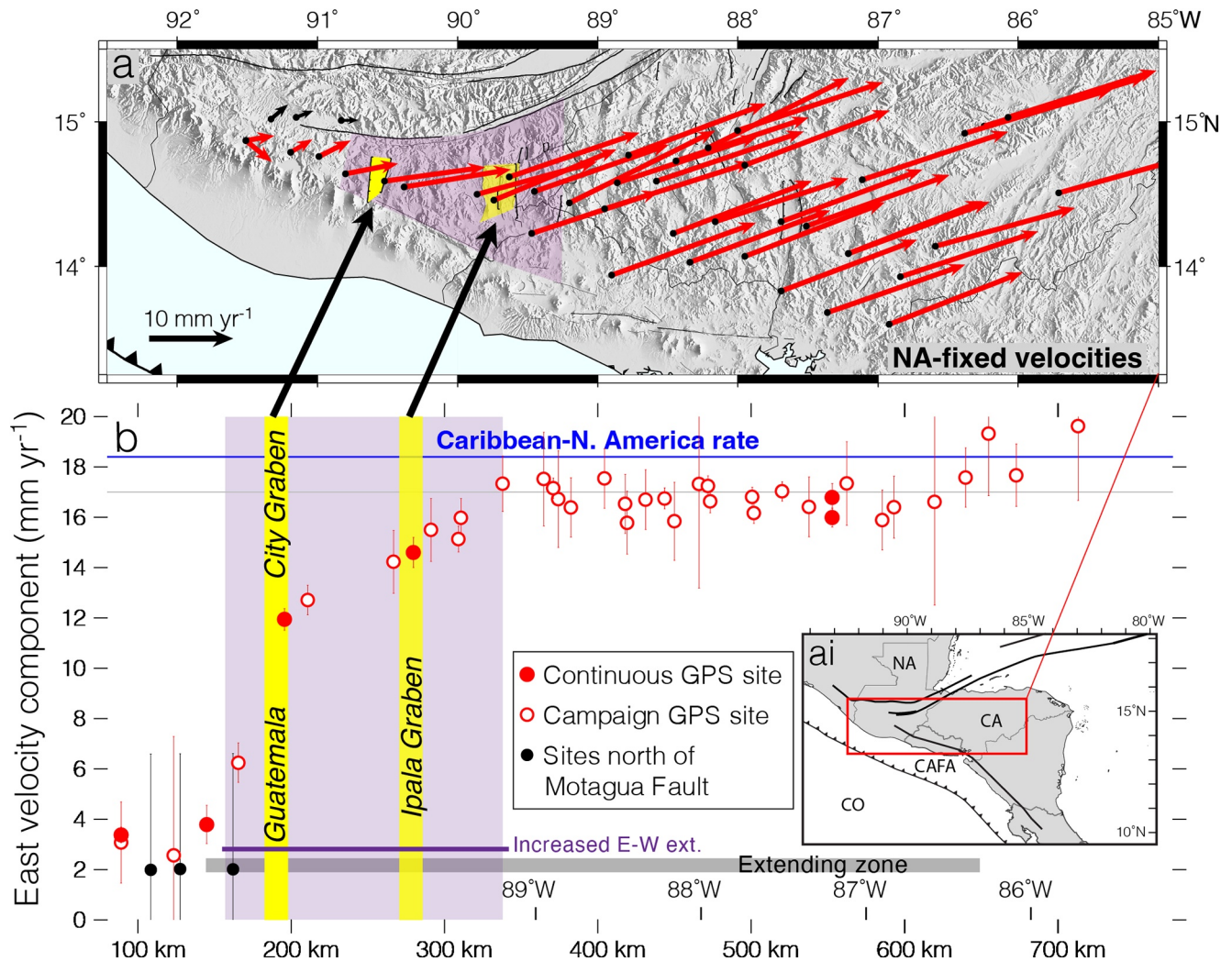


Figure 12. (a) East-to-west transect of measured GPS site velocities relative to the North America plate for the sites depicted in Figure 11. Each measured velocity is corrected for an interseismic elastic velocity component due to the locked faults in our updated elastic block model discussed in this article. The site velocities should thus closely approximate the long-term velocity field. (a). Small inset map in panel (b) shows the location of (a) in the larger context of Central America; NA, North America plate; CA, Caribbean plate; CAFA, Central American Forearc; and CO, Cocos plate. (b) East velocity components for sites from Panel (a) vs. west-to-east distance across the transect. The filled and open red circles show continuous and campaign site rates, respectively. The rates indicated by the black circles show the rates for three sites north of the Motagua Fault (indicated by the black velocity arrows in Panel (a)). All uncertainties are 1-sigma. The blue line indicates the E-W component of Caribbean-North America plate motion estimated with our elastic model along the transect. The gray line displays the extent of the extending zone between the stable Caribbean plate in Honduras and the consistent velocities of the western Guatemala wedge. The purple shaded region defines the zone of increased E-W extension.

uncertainties. For example, the numerous GPS sites in eastern Guatemala and central/western Honduras move 1.5–2 mm/yr westward relative to the Caribbean plate (Figures 10 and 12), consistent with the existence of an independent Chortis Block (Ellis et al., 2019).

The new model predicts similar (albeit faster) slip rates along the Polochic fault; 3.7 ± 1.2 mm/yr vs. 3.2 ± 1.3 mm/yr in the Ellis et al. (2019) model as shown in Figure SA.2 in Supporting Information S1. This result reinforces the interpretation that significant motion occurs between the North America plate and the lithosphere immediately south of the Polochic fault. By implication, the GPS sites immediately west of the Guatemala City graben move significantly (though slowly) relative to the North America plate. In western El Salvador and southern Guatemala, where new measurements have improved the accuracy of GPS site velocities, the better-constrained east-to-west deformation-rate gradient provides a stronger foundation for interpreting our structural data than was previously possible.

Differences between the interseismic locking that is estimated by both models along the Middle America subduction zone and other faults in the model are also small (Figure SA.3 in Supporting Information S1). Both

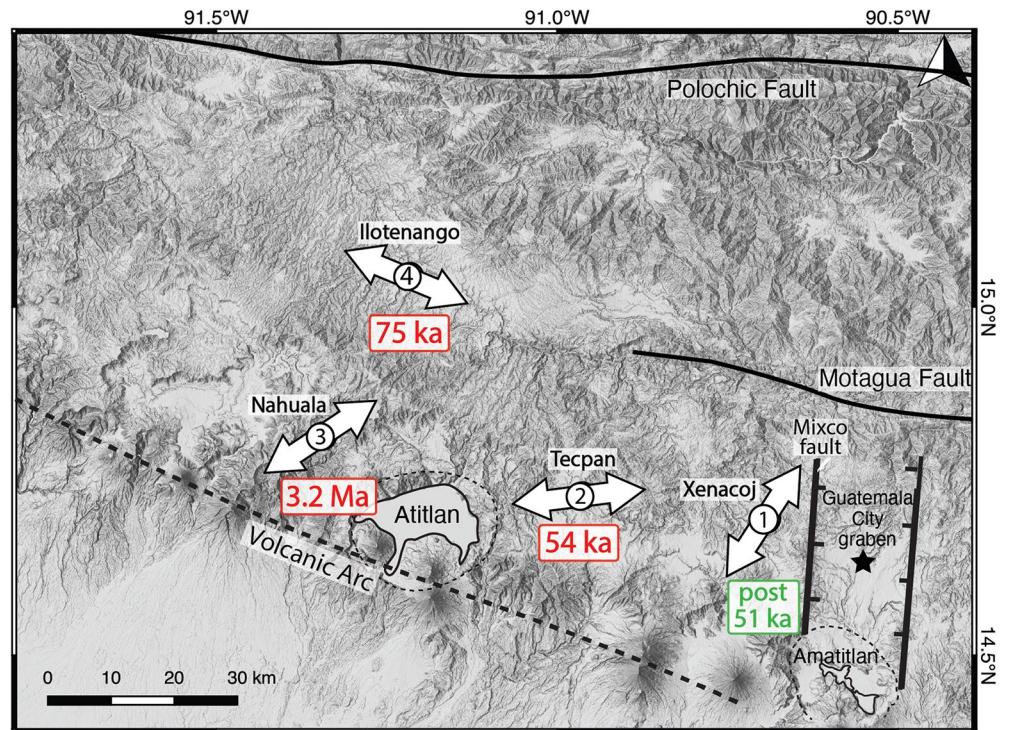


Figure 13. Results from the minor fault analysis of western Guatemala. Arrows display the orientation of maximum elongation estimated for each location based on collected normal fault data. Below each location is the age of fault cessation. Star represents location of Guatemala City.

models indicate that weak locking occurs offshore El Salvador and northwestern Nicaragua, averaging ~15%. Both models also indicate that a transition occurs northwestward along the trench offshore Chiapas, Mexico. The weak subduction zone locking offshore Guatemala transitions to moderate-to-strong subduction zone locking in southernmost Mexico (averaging 65%–70% locking; Ellis et al., 2019).

Long-term velocities in our study area as estimated with the updated elastic block model are due to steady plate and block rotations (Table S2). Long-term distributed deformation within the Chortis, Ipala, and Fonseca blocks clearly define the differing block motions (Figure 10a). The linear block velocities at the location of the Guatemala City graben (Figure 10b) characterize how the movement between the Caribbean and North America plates is partitioned by motions of the Chortis, Ipala, and Motagua-Polochic blocks between the two plates. The relative motions of these blocks and the CAFA define the kinematic framework for our interpretation of deformation at the continental triple junction where the North America, CAFA, and Caribbean plates meet (Section 5.1).

In addition to the material that is presented herein, we refer readers to Ellis et al. (2019), Garnier et al. (2020), and Legrand et al. (2020) for information about the geodetic constraints on the tectonics elsewhere in northern Central America and southern Mexico.

5. Discussion

Geologic and geophysical data has always been scarce in western Guatemala, an area that is important in understanding the tectonics of northern Central America. The goal of our study is to improve this data problem, and use the geodetic and structural data to understand what is currently happening in western Guatemala in the larger tectonic framework, how deformation has changed over time, and how our data compares to previously proposed tectonic models. In a broader context, the results presented here improve our understanding of the deformation that can occur at extensional terminations of tectonic plates or fault blocks, particularly how discrete boundaries can form from distributed deformation. This tectonic setting is unique with an onshore triple junction and prominent moving forearc sliver.

5.1. Geodetic Framework for the NAFCA (North America-CAFA-Caribbean) Triple Junction

Previous studies defined the western Guatemala wedge as part of the Caribbean plate (Álvarez-Gómez et al., 2008; Authemayou et al., 2011; Franco et al., 2012; Guzmán-Speziale et al., 1989; Lyon-Caen et al., 2006; Rodríguez et al., 2009). In contrast, elastic block modeling of the two new velocity fields—given by Ellis et al. (2019) and the updated velocity field presented in this article—indicates that the GPS sites in the western Guatemala wedge (red arrows in Figure 10a and red shaded area in Figure 11) have velocities similar to stations on the CAFA and the North America plate. Specifically, both regional block models indicate that sinistral slip rates across the Polochic-Motagua fault system decrease from 11 to 13 mm/yr just north and west of the Guatemala City graben to 3 mm/yr or less along the Motagua fault directly west of the Guatemala City graben and the Polochic fault at the northern limit of the western Guatemala wedge (Figures 6b and 11 in Ellis et al., 2019). Both models also predict ~7–8 mm/yr of dextral slip along the Jalpatagua fault east and south of the Guatemala City graben, diminishing to ~2 mm/yr of distributed dextral offset between the CAFA and the backarc—with no evidence of a discrete fault—immediately west of the Guatemala City graben (Figure 7b in Ellis et al., 2019; and Figure 9b in Garnier et al., 2020). Both models thus identify the Guatemala City graben as the western limit of the extending end of the Caribbean plate.

In accord with the above, GPS measurements at >40 sites across southern Guatemala clearly reveal 14 ± 1 mm/yr (95% uncertainty) of ~E-W elongation distributed unevenly across a ~500 km-wide zone (gray bar or extending zone on Figure 12). This zone begins ~40–50 km west of the Guatemala City graben, includes the Guatemala City and Ipala grabens, and terminates to the east across a zone of poorly defined grabens in central Honduras (Figure 12). Within this extending zone, there is increased E-W extension within a 150–200 km-wide zone immediately surrounding the Guatemala City and Ipala grabens (purple bar or zone of increased E-W extension on Figure 12). The updated GPS velocity field (Figures 10 and 11), which is less noisy in our study area than the earlier Ellis et al. (2019) velocity field, reveals two features of particular relevance to this study. First, 10 ± 2 mm/yr or 70% of the total elongation within the ~500-km-wide extending wedge occurs across or within a few tens of km of the Guatemala City graben. Second, the E-W elongation rate west of the Guatemala City graben slows dramatically to only 2–3 mm/yr within 50 km west of the graben (Figure 12). No discernible E-W-oriented elongation is found farther west. Additionally, elongation immediately east of the Guatemala City graben appears evenly distributed for ~140 km, seen as a linear slope in velocities within the purple-shaded area, and is not only concentrated within the Ipala graben (Figure 12). The GPS data thus suggest that there is no significant stretching/elongation within the western Guatemala wedge at distances greater than 40–50 km west of the Guatemala City graben (Figure 12). Rather, the wedge moves 3–5 mm/yr relative to the CAFA across the volcanic arc (Figure 10), although not along any discrete fault, and relative to North America across the western Polochic fault. A similar relationship is observed in the recorded earthquake focal mechanisms between the Polochic-Motagua fault system and the volcanic arc. Multiple earthquake focal mechanisms indicating strike-slip and normal rupture have been recorded near the Guatemala City graben and to the east, but only one strike-slip earthquake focal mechanism was recorded west of the extending zone, most likely related to the western termination of the Motagua fault (Álvarez-Gómez et al., 2019; Authemayou et al., 2011).

Based on the geodetic results described above, the Guatemala City graben region, including the surrounding area of diffuse E-W extension, approximates the present triple junction between the North America, CAFA, and Caribbean plates, which we refer to below as the NAFCA triple junction. Because the CAFA separates the Caribbean and Cocos plates everywhere southeast of the Guatemala City graben (i.e., the westernmost limit of the Caribbean plate), the Cocos and Caribbean plates cannot share a triple junction with North America. To a first order, the appropriate plate geometry for northern Central America consists of distinct North America and Caribbean plates and the CAFA sliver that meet at the NAFCA triple junction. Ellis et al. (2019) additionally describe geodetic evidence for two additional continental blocks, the Chortis and Ipala blocks, which are included as part of the westernmost Caribbean plate in our simpler plate geometry.

The concept of the NAFCA triple junction highlights the key role of the CAFA in Central American tectonics. Our updated GPS velocity field shows that the motion of the CAFA relative to the North America plate increases toward the southeast. Relative motion (red arrows in Figure 11, NA-plate reference frame) increases from little-to-no motion in southern Mexico, where the two plates converge along a poorly understood, presumably broad boundary (also see Álvarez-Gómez et al., 2008, 2019), to ~10 mm/yr of northeastward movement in CAFA sites in central and eastern El Salvador (Figure 11). The counterclockwise rotation of the CAFA in Guatemala is

visible in our velocity field as an increase in northeastward-directed velocities along the CAFA to the southeast. This rotation is also visible in the long-term velocities (CA-plate reference frame) as WNW-directed velocities at the southeastern end of the CAFA sweep to WSW-directed velocities near the border with Mexico (Figure 10a). The rotation of this section may be due to the progressively faster eastward movement of the Caribbean plate relative to the North America plate east of the Guatemala City graben. Due to its wedge-shaped geometry, a gap will form south of the Caribbean plate as it moves eastward, constrained by the Motagua fault to the north and the CAFA/volcanic arc boundary to the south. This situation is equivalent to slightly closing the jaws of an open set of pliers; the two sides must move closer together. By analogy, the CAFA/volcanic arc must move inland as the space south of the wedge is created (Figure 10). Therefore, increased eastward velocity of the Caribbean plate will create more space, resulting in a faster NE-directed CAFA velocities.

5.2. Timing of Fault Cessation

Combining the deformational histories of all four outcrops, faulting is oldest in the west and youngest in the east across the western Guatemala wedge (Figure 13). Faulting at Nahualá near the volcanic arc suggests that the western Guatemala wedge was actively deforming in the Pliocene, with fault cessation by ~ 3.2 Ma. The faulting at the Xenacoj outcrop also suggests active deformation in the wedge during the early Pleistocene, with movement of the main fault during deposition of the 1.495 Ma and the 1.145 Ma tephra. After these faulting events, we observe an eastward trend of fault cessations. Faulting ceased by 75 ka (Los Chocoyos ash) at Ilotenango, our western most outcrop, by 54 ka (C tephra) at the central Tecpan outcrop, and faulting may still be active at the eastern most Xenacoj outcrop, as the main fault offsets the 51 ka E tephra and the youngest observed tephra (Figure 13). The record of fault cessations progresses eastward, toward the Guatemala City graben.

5.3. Elongation Directions Determined by Fault Arrays

From east to west, the minor fault analysis estimated NE-directed elongation (033°) at Xenacoj, nearly E-W elongation (083°) at Tecpan, NE elongation (056°) at Nahualá, and ESE elongation (112°) at Ilotenango (Figure 13). The maximum elongation directions are variable, but can be separated into roughly E-W (Tecpan and Ilotenango) and NE-SW (Nahualá and Xenacoj) elongation directions.

While fault data from Tecpan and Ilotenango come from statistically different fault populations (Figure 6), we suggest that they both result from internal E-W elongation of the western Guatemala wedge. E-W elongation at Tecpan is most similar to active E-W elongation directions recorded in secondary faulting along the Jalpatagua fault to the east, as well as E-W extension observed in the GPS data across central and eastern Guatemala, with a majority of the extension concentrated on the Guatemala City graben (Ellis et al., 2019; Garnier et al., 2020).

The similar elongation directions could suggest that the western limit of the Caribbean plate, the limit of active E-W elongation, extended into western Guatemala in the past. If so, elongation was active on both sides of the Guatemala City graben, whereas now it is focused primarily in the graben, as well as immediately to its west and the region to its east including the Ipala graben. While the maximum elongation direction at Ilotenango is more inclined to the ESE, the deformation can still be linked to internal E-W elongation of the Caribbean plate if we account for the curvature of the Motagua-Polochic fault system. While the Motagua and Polochic faults are individually oriented E-W across central and western Guatemala, the fault system appears to create a curved form in map view. That is, the faults collectively create a WNW-oriented curve in western Guatemala; the Motagua fault connects to the Polochic fault to enclose the crescent-shaped block between the two faults, and an ENE-oriented end in eastern Guatemala/western Honduras (Figure 1). Work by Burkart and Self (1985) and modeling by Rodriguez et al. (2009) suggest that elongation directions within the Caribbean plate south of the fault system will parallel and rotate around this curvature as the Caribbean plate moves eastward. This idea is supported by N-S grabens in central Guatemala and NW-trending grabens and faults in western Honduras (Rogers et al., 2002; Rogers & Mann, 2007), and would explain the NE-trending river valleys and faults and the related ESE elongation estimated at Ilotenango within the western Guatemala wedge.

NE-elongations at the Nahualá and Xenacoj outcrops are interpreted differently. NE-oriented elongation (056°) observed at Nahualá is similar to NE-elongations (ranging from 033° to 073°) observed near the eastern

termination of the Jalpatagua fault (Garnier et al., 2020) and within areas of the El Salvador fault zone (Garibaldi et al., 2016). In both cases, the NE-oriented elongations result from distributed deformation associated with dextral, possibly transtensional forearc movement (Garibaldi et al., 2016; Garnier et al., 2020). Since the Nahualá outcrop is near the CAFA boundary, a similar area of oblique divergence could have occurred in the past along the volcanic arc west of the Guatemala City graben. The distributed zones of deformation in El Salvador occur between adjacent strike-slip faults (e.g., Garibaldi et al., 2016; Martínez-Díaz et al., 2021). Since the distributed deformation of this area is similar to the zones within the El Salvador fault zone, it suggests that a dextral fault—an extension of the active Jalpatagua fault—once continued further westward along the south side of the western Guatemala wedge within the active volcanic arc.

The NE-directed maximum elongation orientation (033°) at the Xenacoj outcrop is slightly different from Nahualá, but suggests elongation of the backarc toward the trench, perpendicular to the Motagua-Polochic fault system and volcanic arc. Ritchie (1975) mapped other large faults of this orientation in the area, indicating that the Xenacoj outcrop represents a consistent deformation pattern for the larger area. However, this deformation is also very close, yet highly oblique, to E-W elongation across the Guatemala City graben, making Xenacoj more difficult to connect with other deformational patterns observed across southern Guatemala. With the western termination of the Motagua fault nearby, it is possible that faulting is related to the termination of this structure.

Overall, the elongation directions at Tecpan, Ilotenango, and Nahualá in the western Guatemala wedge parallel active elongations directions estimated in central and eastern Guatemala. With this evidence, we suggest that the internally deforming, trailing end of the Caribbean plate extended into western Guatemala when the extensional faulting took place.

5.4. Comparison of Structural and Geodetic Strain Rates

While many assumptions were made to estimate elongation and elongation rates at all four outcrops (e.g., down-dip movement on faults; period of active faulting), we can still compare the elongation rates to the current GPS study to infer about the past state of deformation. The GPS data indicate that the trailing end of the Caribbean plate is internally deforming at E-W elongation rates of 10 mm/yr across the Guatemala City graben and a slower, constant rate surrounding the graben and into eastern Guatemala, which includes but is not limited to the Ipala graben (pink region in Figure 14c; Ellis et al., 2019; Garnier et al., 2020). The estimated, ESE-directed elongation rate for past deformation (Neogene to 75 ka) in the Ilotenango/linear river valley region (1.2–2.5 mm/yr) is similar to the current distributed rate measured at locations in eastern Guatemala, such as ~ 2 mm/yr across the Ipala graben and the general diffuse deformation in eastern Guatemala (Figure 12). The similarity between these elongation rates supports a connection between past deformation in western Guatemala and current deformation in eastern Guatemala based on data other than fault orientation, supporting that the distributed deformation we observe today could have extended into western Guatemala in the past. It is important to emphasize that our lack of more precise fault timing means that all past elongation rates are minimums and true elongation rates could have been higher. The Ilotenango elongation rate is estimated for a large region of distributed deformation, similar to the current situation of distributed elongation east of the Guatemala City graben (purple-shaded region in Figure 12). While deposition ages are better constrained at Tecpan, the E-W elongation rate of 0.063 mm/yr is much smaller than the current elongation rates across the large grabens. However, Tecpan could indicate the lower end of E-W strain rates across minor structures or small areas.

The slow elongation rates estimated from Xenacoj (0.007 mm/yr) and Nahualá (~ 0.001 mm/yr) likely underestimate the strain rate needed to create the observed deformation, particularly the extensive faulting at Xenacoj. The lack of precise ages for reworked deposits that would more accurately constrain rate estimates make it difficult to compare to the GPS data. However, the current GPS data observes 2–3 mm/yr of E-W extension within 50 km west of the Guatemala City graben, which includes the Xenacoj outcrop. This observation supports our observation that the main fault cuts all deposits, including the most recent Amatitlán tephra, and faulting is still active in this area.

Estimated elongation and elongation rates in western Guatemala suggest that the Polochic fault and the volcanic arc were active structures during the period of active faulting. Currently, there is 2–4 mm/yr of sinistral

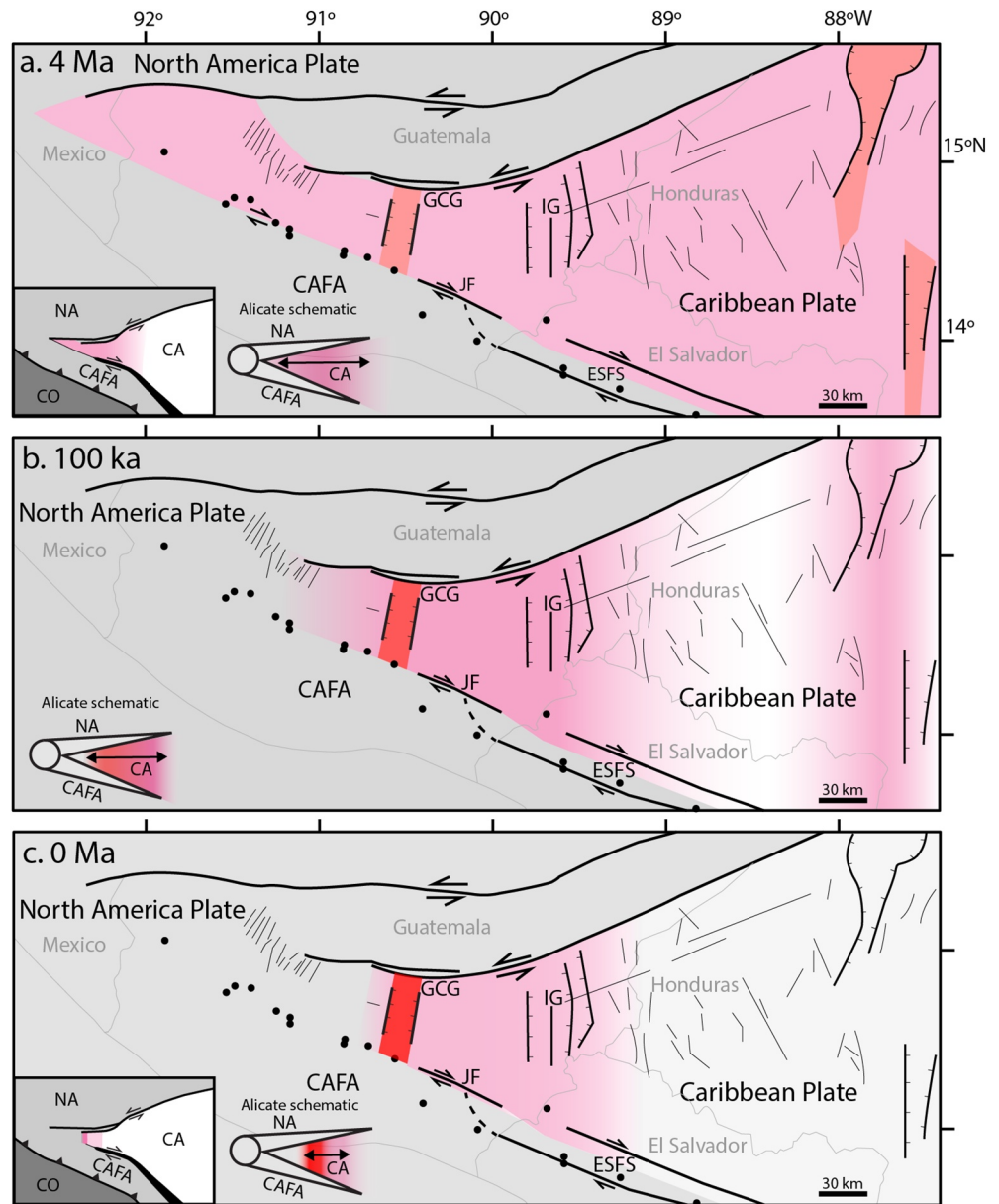


Figure 14. Model of time progressive strain localization in the Caribbean wedge since 4 Ma. Color schematically indicates relative strain intensity. Abbreviations: NA, North America plate; CA, Caribbean plate; CAFA, Central American Forearc; CO, Cocos plate; GCG, Guatemala City graben; IG, Ipala graben; JF, Jalpatagua fault; ESFS, El Salvador fault system. (a) 4 Ma (upper panel): Distributed ~east-west elongation took place across major grabens and numerous minor faults from western Guatemala to western Honduras. Inset maps show schematics of the larger tectonic system (left) and the system within the alicate (pliers) analogy (right) during this time period with a broad extending region indicated with pink. (b) 100 ka (middle panel): Strain localized toward the Guatemala City and Ipala grabens, ceasing movement on minor structures in western Guatemala, and in turn, transferring western Guatemala to the North America plate and stabilizing the volcanic arc. Inset map shows the alicate schematic of this time period with strain localizing within a narrower extending region as the upper panel, indicated with darker pink/red. (c) 0 Ma (lower panel): East-west elongation is only observed across the Guatemala City graben and the Ipala graben, to a lesser extent. Deformation on minor structures has ceased. The Guatemala City graben is the western boundary between the North America and Caribbean plates. Inset maps show the schematics of the larger tectonic system (left) and the system viewed within the alicate analogy (right) with strain localized within a bounded extending zone (red).

movement estimated for the Polochic fault to the north (e.g., Ellis et al., 2019), but it is unclear if a higher rate could have been present, or required, during the past (further interpretations of earlier slip rates of the Polochic fault presented in Authemayou et al., 2012). To the south, there is minor differential velocity between the CAFA and the backarc within the area 40–50 km west of the Guatemala City graben. The lack of discrete faults on the north side of the CAFA in this area indicates that this difference is not due to discrete dextral motion across the volcanic arc west of the Guatemala City graben (Figure 11; Ellis et al., 2019). Previous authors have mapped fragmented lineaments parallel to the CAFA boundary across the volcanic arc, but most are buried by the nearby volcanic centers and their deposits (Newhall, 1987). Additionally, minor fault orientations recorded within the Atitlán caldera are similar to minor fault sets measured along the active CAFA boundary in eastern Guatemala, the Jalpatagua fault (i.e., N-striking normal faults and strike-slip fault sets following the Riedel shear model for dextral shear; Garnier et al., 2020; Newhall, 1987). Minor faulting indicative of major dextral movement and the presence of the Atitlán caldera (known to have three large caldera-forming events) along the now stable volcanic arc may support past motion along this boundary, as calderas could have been connected to movement on large strike-slip faults (Garibaldi et al., 2016; Saxby et al., 2016; Suñe-Puchol et al., 2019).

5.5. Geologic Evidence for the NAFCA Triple Junction

The Guatemala City graben region is the current plate juncture between the North America, CAFA, and Caribbean plates (e.g., Ellis et al., 2019). The sinistral Motagua-Polochic fault system forms the main boundary between the North America and Caribbean plates. Within this system, two thirds or more of the slip occurs on the Motagua fault, which ends ~25 km west of the Guatemala City graben. There is abundant evidence of normal faulting south of the Motagua fault near the western end of the Caribbean plate (Langer & Bollinger, 1979), including at the Xenocoj outcrop.

Another way of evaluating the movement of the western Guatemala wedge is to investigate its relation to the forearc. The dextral Jalpatagua fault in southeastern Guatemala is the main boundary between the Caribbean plate and the CAFA. The western termination of the Jalpatagua fault occurs at or near the Amatitlán caldera, at the southern end of the Guatemala City graben (Garnier et al., 2020). There is no structure or geomorphic evidence for an active fault that could be the continuation of the Jalpatagua fault west of the Amatitlán caldera/Guatemala City graben. Therefore, both of the major Caribbean plate boundaries in Guatemala—the Motagua and Jalpatagua faults—have geologic evidence of terminations near the Guatemala City graben. Hence, the geologic and geodetic data indicate that the Guatemala City graben and faulting immediately west of the graben are the current western limit of the Caribbean plate. The Motagua and Jalpatagua faults, with opposing shear senses, act as slip margins that allows the Caribbean plate to move eastward. E-W-directed deformation at the western end of the Caribbean plate accommodates the space or gap that is created as the Caribbean plate moves eastward constrained by the North America and CAFA plate boundaries. Since a majority of the eastward movement is accommodated across the Guatemala City graben, with distributed extension surrounding the graben from just to its west to eastern Guatemala, the evidence supports that the Guatemala City graben *region* currently acts as the NAFCA triple junction. The geodetic evidence for several mm/yr of slip along the western Polochic fault (Figure SA.2 in Supporting Information S1 and Section 4.5), which detaches the North America plate from the lithosphere immediately west of the Guatemala City graben, and modeling of the independent Chortis and Ipala blocks clearly show that the Guatemala City graben is not a discrete NAFCA triple junction. Rather, the Guatemala City graben is the primary active structure within a broader deforming region that accommodates the present movement between the three major plates.

Although the sinistral Motagua and Polochic faults jointly accommodate North America-Caribbean plate relative motion (Figure 1), the former ends in an extensional zone to the south and the latter in a contractional zone to the north. From a North American perspective, the Motagua fault allows eastward movement of the westernmost Caribbean plate (Figure 12, Ellis et al., 2019; Lyon-Caen et al., 2006). Nearing central Guatemala, slip along the Motagua fault decreases rapidly as the fault slip is transferred southward onto extensional faults of eastern and central Guatemala, the western end of the Caribbean plate. In contrast, slip on the Polochic fault diminishes more gradually westward (Ellis et al., 2019), and the fault motion is partitioned northward onto thrust and strike-slip faults in the diffuse shortening zone of southern Mexico and northern Guatemala (e.g., Guzmán-Speziale, 2001, 2010). Thus, internal deformation of the North America plate at least partly accommodates the termination of the Polochic fault.

5.6. Progressive Localization and Trailing Edge “Capture”

With the current western limit of the Caribbean plate occurring near the Guatemala City graben, the evidence discussed above supports that the western limit of the Caribbean plate extended into western Guatemala in the past (Figure 14). Strain distributed across small structures ceased toward the Guatemala City graben over 100 ka or more, which differs from the predicted western Guatemala deformation from previous triple junction models. We propose an updated model for plate interactions where distributed strain is localized over time toward the Guatemala City graben. Thus, the eastward movement of the trailing edge of the Caribbean plate sequentially sutures western Guatemala to the CAFA, as the western limit of this strain migrates eastward (Figure 14).

Figure 14 forms the basis for our “alicate” (ah-lee-KHAH-tay) strain localization model for NAFCA plate interactions from ~4 Ma to present. Alicate is Spanish for pliers, which is a good geometric visual for the NAFCA plate system and shares some mechanical similarities. In terms of geometry, the North America plate and the CAFA create the top and bottom jaws of a pair of needle-nose pliers, with the fulcrum near the Mexico/Guatemala border where the western termination of the Polochic fault and volcanic arc meet (Figure 14a). The western Caribbean plate is the wedge-shaped space between the plier jaws.

During the Pliocene and part of the Pleistocene, the deforming end of the Caribbean plate extended from western Guatemala to western Honduras, a larger area than we observe today, and underwent east-west elongation between the volcanic arc and the Polochic-Motagua fault system (Figure 14a). Our evidence of past fault activity in the western Guatemala wedge supports this inference and kinematically requires: (a) the presence of a right-lateral slip—on an arc-parallel fault—that extended further west than the current Jalpatagua fault; and (b) more left-lateral slip on the western end of the Motagua-Polochic system, presumably on the Polochic fault. The area of distributed deformation also extended further to the east, as faults and grabens in western Honduras initiated around 10 Ma and were active after 3.5 Ma (Rogers et al., 2002; Rogers & Mann, 2007) gray fault traces east of the Ipala graben in Figure 14).

In our “alicate” model, the entire western end of the Caribbean plate was extending between the upper (NA) and lower (CAFA) jaws of the pliers, with movement along the entirety of each jaw (Figure 14a). One can imagine this as if the NA/CAFA pliers were applying minimal pressure to the Caribbean plate, only pinning the very tip of the wedge in the fulcrum, and the remaining wedge gently elongated as it moves eastward out of the pliers. This configuration is necessary to explain the consistent extensional deformation observed in western Guatemala at >100 ka before present. During this time, it is unclear where to place the western limit of this spatially extensive deformation.

With evidence of deformation ceasing in an eastward trend in the western Guatemala wedge, we suggest that widespread, distributed strain of the western end of the Caribbean plate progressively localized toward the Guatemala City graben area and eastern Guatemala during the Pleistocene (Guatemala City and Ipala graben; Figures 14b and 14c). It is difficult to pinpoint when this localization began, but possibly over 3 Ma years ago since faulting at Nahualá ceased by 3.2 Ma. Eastward cessation of faulting within the western Guatemala wedge would also track an eastward stabilization of the volcanic arc as dextral motion stopped. As deformation within the wedge and along the volcanic arc ceased in an eastward fashion, inactive material of western Guatemala became essentially sutured to the CAFA. The faults and grabens in western Honduras also became inactive over this time as well (Rogers et al., 2002; Rogers & Mann, 2007), as our GPS site velocities are relatively constant in western Honduras, with little to no E-W-direction elongation/stretching observed between GPS sites (sites east of the purple increased E-W extension zone in Figure 12). However, we do not have evidence that Honduran fault activity ceased in a westward pattern to mirror the eastward pattern observed in western Guatemala. Migration towards the Guatemala City graben from the east and west, strain localizing towards the major structure, is predicted with the alicate model.

The new geodetic results demonstrate that not all strain has currently localized into the Guatemala City graben (Figure 14c). The Guatemala City graben is the most active and western structure of the extending western end of the Caribbean plate, but surrounded by minor distributed deformation as we would expect for a complicated onshore triple junction. Additionally, our current NAFCA plate configuration is most likely over 50 ka old, as faulting at Tecpan ceased by 54 ka.

In our alicate model, the jaws of the pliers closed with continued NA and CA plate movements and counterclockwise rotation of the CAFA, applying increasing pressure to material nearest to the fulcrum, the western Guatemala wedge (transition—Figure 14b, today—Figure 14c). As western Guatemala became increasingly pinned within the fulcrum, no slip along the plier jaws could occur in that area. Therefore, elongation localized toward the nearest and largest points of weakness, the Guatemala City graben and surrounding structures of eastern Guatemala, and the remaining material of the Caribbean plate continued to move out of the pliers. In simple terms, the western Guatemala wedge is stuck in the hinge region of the NA/CAFA pliers and the Caribbean plate breaks off at the Guatemala City graben in order to continue moving eastward.

This process of pinning of the western Guatemala wedge is similar to the Authemayou et al. (2011) zipper model, although different in detail. The Authemayou et al. (2011) zipper model predicts that the Caribbean plate escapes between the North America plate and the CAFA as they suture together. This prediction would result in the juxtaposition of the left-lateral Motagua-Polochic fault and the right-lateral arc-parallel (e.g., Jalpatagua) fault. Our data in western Guatemala does not support this model, as the western Guatemala wedge simply ceased deforming. Rather, the western end of the Caribbean plate progressively transferred, or was captured, to the North America plate and/or CAFA as motion along the volcanic arc and Polochic fault significantly reduced (Figure 7). A similar prediction of material transfer of western Guatemala was made from the recent modeling study from Álvarez-Gómez et al. (2019).

Alternatively, one could consider the alicate model as a variant of the zipper model, but the zipper or pliers never fully close. Instead, more and more material can become pinned between the plier jaws as the CAFA rotates to align with the North America plate. However, the alicate model has more explanatory power because it also recognizes that the extensional structures in Honduras are also progressively abandoned, rather than only a south-eastward trend in the suturing or triple junction. Regardless, the alicate model provides a better description of the recent history (~100 ka, at a minimum) and current motions associated with this triple junction. It is possible that the zipper model of Authemayou et al. (2011) characterizes well the earlier, possibly Miocene, deformation associated with this triple junction.

The ages of the Guatemala City and Ipala grabens are a crucial detail missing from this model. We assume—based on their size, historic seismicity, and current elongation rates—that these structures have been active throughout our described Pliocene and Pleistocene deformation. However, we know of no available information on their ages of initiation, which would be an important area for future research.

As a final point, redefining the Guatemala City graben as the focus of the NAFCA triple junction increases the importance and the perceived earthquake risk of a structure that contains nearly 16% of the country's population. While the people living in the Guatemala City graben have always lived with a risk of destructive earthquakes by its location near the Motagua fault, the location of the historic 1976 earthquake ($M_w = 7.5$), the risk appears much greater now that we suggest that the Guatemala City graben is more like a plate boundary, being the most active and western structure of the larger extensional region. Movement along the nearby Motagua fault (the North America-Caribbean boundary) or the Jalpatagua fault (the CAFA-Caribbean boundary) could trigger additional destructive earthquakes, affecting the graben and the large metropolitan area.

6. Conclusions

Analysis of minor faulting and four new $^{40}\text{Ar}/^{39}\text{Ar}$ dates in western Guatemala indicate that internal deformation of the region was active in the Pliocene and part of the Pleistocene, recording roughly east-west elongation and slight transtension, but has ceased in an eastward trend through time toward the Guatemala City graben. The geologic and geodetic evidence supports that the Guatemala City graben region is the current triple junction between the North America, Central American Forearc, and Caribbean (NAFCA) plates.

The four analyzed outcrops all contain evidence of past faulting. $^{40}\text{Ar}/^{39}\text{Ar}$ dating and unit correlation show that faulting within western Guatemala was active in the Pliocene (Nahualá outcrop) and ceased in an eastward trend: by 75 ka at the westernmost outcrop Ilotenango, by 54 ka in the central Tecpan outcrop, and after 51 ka at the Xenacoj outcrop just west of the Guatemala City graben, for which faulting on the main fault may still be active. Analysis of minor faulting at these outcrops indicate E-W and ESE-directed elongation occurred at the Tecpan

and Ilotenango outcrops, in amounts of 0.64% and 15.8%, respectively. Additionally, NE- and NNE-directed elongation was estimated at the Nahualá and Xenacoj outcrops, in amounts of 4.2%–4.7% and 11.5%, respectively.

The updated velocity field indicates that the Guatemala City graben is the current western extent of the extending end of the Caribbean plate, as the western Guatemala wedge is relatively inactive and moves with the CAFA and/or North America plate. Extensional deformation is focused on the Guatemala City graben, with more distributed extension extending just west of the graben and across eastern Guatemala. Additionally, slip along the north and south-bounding Motagua and Jalpatagua faults, respectively, diminishes and terminates into the Guatemala City graben region.

We hypothesize that during the Pliocene and part of the Pleistocene, the trailing end of the Caribbean plate extended across Guatemala, between the Polochic-Motagua fault system and the volcanic arc/CAFA. Further, this region underwent east-west elongation, and NE-directed transtension, in a distributed fashion across minor and major faults and structures. Elongation ceased on normal faults in western Guatemala as deformation became localized in the Guatemala City graben and surrounding structures including the Ipala graben. The same effect occurred in Honduras adjacent to the Motagua fault, as normal faults no longer accommodate any of the geodetic movement in that region (Ellis et al., 2019). We propose the “alicate” model, in which the Caribbean plate moves eastward in-between the upper and lower jaws of the North America/CAFA pliers. The extensional strain localization into the Guatemala City graben region progressively transferred western Guatemala to the CAFA and/or North America plate. This alicate model of time-progressive strain localization agrees with past deformation observed in western Guatemala and western Honduras and the current GPS velocity model that depicts a North America-CAFA and Caribbean plate boundary that ends at the Guatemala City graben.

Data Availability Statement

To comply with AGU's data policy, fault measurement data is available to download from Strabospot under the project name “Guatemalan Forearc: Bridget Garnier”, rock samples are registered in the IGSN based on the IGSNs in Table 1, geochemical data is available in the Geochem database (Garnier, 2021, <https://doi.org/10.26022/IEDA/112033>), Geodetic data is available from UNAVCO (DeMets & Cosenza-Murales, 2021, <https://doi.org/10.7283/KH2R-K704>), and geochronological data are available in a public GitHub repository. Additionally, data sets are also described in this Ph.D. dissertation (Garnier, 2020; University of Wisconsin-Madison). Original rock samples used in the geochemical and geochronological analyzes supporting this research are available in the geology museum collections at the University of Wisconsin-Madison under UW number UW2045.

References

- Alvarado, D., DeMets, C., Tikoff, B., Hernandez, D., Wawrzyniec, T. F., & Pullinger, C. (2011). Forearc motion and deformation between El Salvador and Nicaragua: GPS, seismic, structural, and paleomagnetic observation. *Lithosphere*, 3(1), 3–21. <https://doi.org/10.1130/L108.1>
- Alvarado Cabrera, G. D., & Herrero Ibáñez, I. R. (2001). *Mapa Fisiográfico-Geomorfológico de la República de Guatemala a escala 1:250,000*. Ganadería y Alimentación: Ministerio de Agricultura.
- Álvarez-Gómez, J. A., Meijer, P. T., Martínez-Díaz, J. J., & Capote, R. (2008). Constraints from finite element modeling on the active tectonics of northern Central America and the Middle America trench. *Tectonics*, 27, TC1008. <https://doi.org/10.1029/2007TC002162>
- Álvarez-Gómez, J. A., Staller Vázquez, A., Martínez-Díaz, J. J., Canora, C., Alonso-Henar, J., Unsua-Arévalo, J. M., & Béjar-Pizarro, M. (2019). Push-pull driving of the Central America Forearc in the context of the Cocos-Caribbean-North America triple junction. *Nature*, 9, 11164.
- Andreani, L., & Gloaguen, R. (2016). Geomorphic analysis of transient landscapes in the Sierra Madre de Chiapas and Maya Mountains (northern Central America): Implications for the North American-Caribbean-Cocos plate boundary. *Earth Surface Dynamics*, 4, 71–102. <https://doi.org/10.5194/esurf-4-71-2016>
- Argus, D. F., Gordon, R. G., & DeMets, C. (2011). Geologically current motion of 56 plates relative to the no-net-rotation reference frame. *Geochemistry, Geophysics, Geosystems*, 12(11), Q11001. <https://doi.org/10.1029/2011GC003751>
- Authemayou, C., Brocard, G., Teyssier, C., Simon-Labric, T., Guittierrez, A., Chiquin, E. N., et al. (2011). The Caribbean-North America-Cocos triple junction and the dynamics of the Polochic-Motagua fault systems: Pull-up and zipper models. *Tectonics*, 30, TC3010. <https://doi.org/10.1029/2010TC002814>
- Authemayou, C., Brocard, G., Teyssier, C., Suski, B., Conenza, B., Morán-Icaal, S., et al. (2012). Quaternary seismo-tectonic activity of the Polochic Fault, Guatemala. *Journal of Geophysical Research*, 117, B07403. <https://doi.org/10.1029/2012jb009444>
- Borchardt, G. A., & Harward, M. E. (1971). Trace element correlation of volcanic ash soils. *Soil Science Society of America Proceedings*, 35, 626–631. <https://doi.org/10.2136/sssaj1971.03615995003500040040x>
- Burkart, B. (1978). Offset across the Polochic fault of Guatemala and Chiapas, Mexico. *Geology*, 6, 328–332. [https://doi.org/10.1130/0091-7613\(1978\)6<328:oatpfo>2.0.co;2](https://doi.org/10.1130/0091-7613(1978)6<328:oatpfo>2.0.co;2)
- Burkart, B. (1983). Neogene North American-Caribbean Plate boundary across northern Central America: Along the Polochic fault. *Tectonophysics*, 99, 251–270. [https://doi.org/10.1016/0040-1951\(83\)90107-5](https://doi.org/10.1016/0040-1951(83)90107-5)

Acknowledgments

This work was funded by the National Science Foundation [grant EAR-1144418 (DeMets)]. The authors thank Guatemalan institutions that provided technical and safety support including University of Guatemala in Coban, INSIVUMEH of Guatemala, and CONRED of Guatemala. Special thanks go to Joshua Rodenas, Roberto Mérida Boogher, Carlos Pérez, and Víctor Pérez, who aided in field work, Sergio Mendez Rojas, Allen Schaen, Bryan Wathen, and Randy Williams, who aided in lab work, and Neal Lord, who was instrumental in the geodetic operations and field work. Additional thanks go to Maximiliano Garnier Villarreal, who named our alicate model. Reviews by Peter LaFemina, two anonymous reviewers, and associate editor Margaret E. Rushmore improved the manuscript.

- Burkart, B., & Self, S. (1985). Extension and rotation of crustal blocks in northern Central America and effect on the volcanic arc. *Geology*, *13*, 22–26. [https://doi.org/10.1130/0091-7613\(1985\)13<22:earoch>2.0.co;2](https://doi.org/10.1130/0091-7613(1985)13<22:earoch>2.0.co;2)
- Cisneros de León, A., Schindlbeck-Belo, J. C., Kutterolf, S., Danišik, M., Schmitt, A. K., Freund, A., et al. (2021). A history of violence: Magma incubation, timing, and tephra distribution of the Los Chocoyos supereruption (Atitlán, Guatemala). *Journal of Quaternary Science*, *36*(2), 169–179.
- Clohan, G. M., & Reynolds, J. C. (1977). *The geology of the eastern portion of the Sololá quadrangle, Guatemala*, (Undergraduate thesis, p. 72). Dartmouth College.
- Correa-Mora, F., DeMets, C., Alvarado, D., Turner, H. L., Mattioli, G. S., Hernandez, D., et al. (2009). GPS-derived coupling estimates for the Central America subduction zone and volcanic arc faults: El Salvador, Honduras, and Nicaragua. *Geophysical Journal International*, *179*, 1279–1291. <https://doi.org/10.1111/j.1365-246x.2009.04371.x>
- Cronin, V. S. (1992). Types and kinematic stability of triple junctions. *Tectonophysics*, *207*, 287–301. [https://doi.org/10.1016/0040-1951\(92\)90391-i](https://doi.org/10.1016/0040-1951(92)90391-i)
- Davis, J. R., & Titus, S. J. (2017). Modern methods of analysis for three-dimensional orientational data. *Journal of Structural Geology*, *96*, 65–89.
- DeMets, C., & Cosenza-Murales, B. (2021). Central America 2018—Guatemala—GPS/GNSS Observations data set. UNAVCO. <https://doi.org/10.7283/KH2R-K704>
- DeMets, C., Gordon, R. G., & Argus, D. F. (2010). Geologically current plate motions. *Geophysical Journal International*, *181*, 1–80. <https://doi.org/10.1111/j.1365-246X.2009.04491.x>
- Drexler, J. W., Rose, W. I., Sparks, R. S. J., & Ledbetter, M. T. (1980). The Los Chocoyos ash, Guatemala: A major stratigraphic marker in Middle America and in three oceans basins. *Quaternary Research*, *13*, 327–345. [https://doi.org/10.1016/0033-5894\(80\)90061-7](https://doi.org/10.1016/0033-5894(80)90061-7)
- Eggert, R. G., & Lea, P. D. (1978). *The geology of the central portion of the Santa Catarina Ixtahuacan quadrangle, Guatemala* (Undergraduate thesis, p. 86). Dartmouth College.
- Ellis, A. P., DeMets, C., Briole, P., Cosenza, B., Flores, O., Graham, S. E., et al. (2018). GPS constraints on deformation in northern Central America from 1999 to 2017, Part 1—Time-dependent modeling of large regional earthquakes and their post-seismic effects. *Geophysical Journal International*, *214*, 2177–2194. <https://doi.org/10.1093/gji/ggy249>
- Ellis, A. P., DeMets, C., Briole, P., Cosenza, B., Flores, O., Graham, S. E., et al. (2019). Deformation in northern Central America from 1999 to 2017 using GPS observations, Part 2: Block rotations, fault slip rates, fault locking, and distributed deformation. *Geophysical Journal International*, *218*, 729–754. <https://doi.org/10.1093/gji/ggz173>
- Franco, A., Lasserre, C., Lyon-Caen, H., Kostoglodov, V., Molina, E., Guzman-Speziale, M., et al. (2012). Fault kinematics in northern Central America and coupling along the subduction interface of the Cocos Plate, from GPS data in Chiapas (Mexico), Guatemala and El Salvador. *Geophysical Journal International*, *189*, 1223–1236. <https://doi.org/10.1111/j.1365-246x.2012.05390.x>
- Garibaldi, N., Tikoff, B., & Hernández, W. (2016). Neotectonic deformation within an extensional stepover in El Salvador magmatic arc, Central America: Implication for the interaction of arc magmatism and deformation. *Tectonophysics*, *693*, 327–339. <https://doi.org/10.1016/j.tecto.2016.05.015>
- Garnier, B. (2020). *Faulting in southern Guatemala and implications for the North America-forearc-Caribbean triple junction*, (Ph.D. thesis). University of Wisconsin-Madison.
- Garnier, B. (2021). XRF data from samples collected across southern Guatemala, 2014–2019: Version 1.0. *Interdisciplinary Earth Data Alliance (IEDA)*. <https://doi.org/10.26022/IEDA/112033>
- Garnier, B., Tikoff, B., Flores, O., Jicha, B., DeMets, C., Cosenza-Murales, B., et al. (2020). An integrated structural and GPS study of the Jalpatagua Fault, Southeastern Guatemala. *Geosphere*, *17*, 1–25. <https://doi.org/10.1130/ges02243.1>
- Gordon, M., & Muehlberger, W. R. (1994). Rotation of the Chortis block causes dextral slip on the Guayape fault. *Tectonics*, *13*(4), 858–872. <https://doi.org/10.1029/94tc00923>
- Gross, M. R., & Engelder, T. (1995). Strain accommodated by brittle failure in adjacent units of the Monterey Formation, U.S.A.: Scale effects and evidence for uniform displacement boundary conditions. *Journal of Structural Geology*, *17*(9), 1303–1318. [https://doi.org/10.1016/0191-8141\(95\)00011-2](https://doi.org/10.1016/0191-8141(95)00011-2)
- Guzmán-Speziale, M. (2001). Active seismic deformation in the graben of northern Central America and its relationship to the relative motion of the North America-Caribbean plate boundary. *Tectonophysics*, *337*, 39–51.
- Guzmán-Speziale, M. (2010). Beyond the Motagua and Polochic faults: Active strike-slip faulting along the Western North America-Caribbean plate boundary zone. *Tectonophysics*, *496*, 17–27. <https://doi.org/10.1016/j.tecto.2010.10.002>
- Guzmán-Speziale, M., Pennington, W. D., & Matumoto, T. (1989). The triple junction of the North America, Cocos, and Caribbean plates: Seismicity and tectonics. *Tectonics*, *8*(5), 981–997.
- Holekamp, C. P., Larson, J. E., & Lundstrom, S. C. (1978). *The geology of the adjoining portions of the Santa Catarina Ixtahuacán and Sololá quadrangles, Guatemala*, (Undergraduate thesis, p. 47). Dartmouth College.
- Hughes, J. M. (1978). *Geology and petrology of Caldera Tzanjuyub, western Guatemala*, (MS thesis) (p. 129). Dartmouth College.
- Jicha, B. R., Singer, B. S., & Sobol, P. (2016). Re-evaluation of the ages of ⁴⁰Ar/³⁹Ar sanidine standards and supereruptions in the western U.S. using a Noblesse multi-collector mass spectrometer. *Chemical Geology*, *431*, 54–66. <https://doi.org/10.1016/j.chemgeo.2016.03.024>
- Kobayashi, D., LaFemina, P., Geirsson, H., Chichaco, E., Abrego, A. A., Mora, H., et al. (2014). Kinematics of the western Caribbean: Collision of the Cocos Ridge and upper plate deformation. *Geochemistry, Geophysics, Geosystems*, *15*, 1671–1683. <https://doi.org/10.1002/2014gc005234>
- Koch, A. J. (1970). *Stratigraphy, petrology, and distribution of Quaternary pumice deposits of the San Cristobal group, Guatemala City Area, Guatemala*, (Ph.D. thesis). University of Washington.
- Koch, A. J., & McLean, H. (1975). Pleistocene and tephra and ash-flow deposits in the volcanic highlands of Guatemala. *GSA Bulletin*, *86*, 529–541. [https://doi.org/10.1130/0016-7606\(1975\)86<529:ptaadi>2.0.co;2](https://doi.org/10.1130/0016-7606(1975)86<529:ptaadi>2.0.co;2)
- LaFemina, P., Dixon, T. H., Govers, R., Norabuena, E., Turner, H., Saballos, A., et al. (2009). Fore-arc motion and Cocos Ridge collision in Central America. *Geochemistry, Geophysics, Geosystems*, *10*(5), Q05S14. <https://doi.org/10.1029/2008GC002181>
- Langer, C. J., & Bollinger, G. A. (1979). Secondary faulting near the terminus of a seismogenic strike-slip fault: Aftershocks of the 1976 Guatemala Earthquake. *Bulletin of the Seismological Society of America*, *69*(2), 427–444. <https://doi.org/10.1785/bssa0690020427>
- Legrand, D., Marroquín, G., DeMets, C., Mixco, L., García, A., Villalobos, M., et al. (2020). Active deformation in the San Salvador extensional stepover, El Salvador from an analysis of the April–May 2017 earthquake sequence and GPS data. *Journal of South American Earth Sciences*, *104*, 102854. <https://doi.org/10.1016/j.jsames.2020.102854>
- Lyon-Caen, H., Barrier, E., Lasserre, C., Franco, A., Arzu, I., Chiquin, L., et al. (2006). Kinematics of the North America-Caribbean-Cocos plates in Central America from new GPS measurements across the Polochic-Motagua fault system. *Geophysical Research Letters*, *33*, L19309. <https://doi.org/10.1029/2006gl027694>
- Marrett, R., & Allmendinger, R. W. (1991). Estimates of strain due to brittle faulting: Sampling of fault populations. *Journal of Structural Geology*, *13*(6), 735–738. [https://doi.org/10.1016/0191-8141\(91\)90034-g](https://doi.org/10.1016/0191-8141(91)90034-g)

- Marrett, R., & Allmendinger, R. W. (1992). Amount of extension on “small” faults: An example from the Viking graben. *Geology*, *20*, 47–50. [https://doi.org/10.1130/0091-7613\(1992\)020<0047:aeosf>2.3.co;2](https://doi.org/10.1130/0091-7613(1992)020<0047:aeosf>2.3.co;2)
- Martínez-Díaz, J. J., Álvarez-Gómez, J. A., Staller, J., Alonso-Henar, J., Canora-Catalán, C., Insúa-Arévalo, J. M., et al. (2021). Active fault of El Salvador. *Journal of South American Earth Sciences*, *125*(103038).
- McKenzie, D. P., & Morgan, W. J. (1969). Evolution of triple junctions. *Nature*, *224*, 125–133. <https://doi.org/10.1038/224125a0>
- McLean, H. (1970). *Stratigraphy, mineralogy, and distribution of the Sumpango group pumice deposits in the volcanic highlands of Guatemala*. (Ph.D. thesis, p. 99). University of Washington.
- Min, K., Mundil, R., Renne, P. R., & Ludwig, K. R. (2000). A test for systematic errors in $^{40}\text{Ar}/^{39}\text{Ar}$ geochronology through comparison with U/Pb analysis of a 1.1-Ga rhyolite. *Geochimica et Cosmochimica Acta*, *64*(1), 73–98.
- Morgan, W. J. (1968). Rises, trenches, great faults, and crustal blocks. *Journal of Geophysical Research*, *73*(6), 1959–1982. <https://doi.org/10.1029/jb073i006p01959>
- Muehlberger, W. R., & Ritchie, A. W. (1975). Caribbean-Americas plate boundary in Guatemala and southern Mexico as seen on Skylab IV orbital photography. *Geology*, *3*, 232–235. [https://doi.org/10.1130/0091-7613\(1975\)3<232:cpbiga>2.0.co;2](https://doi.org/10.1130/0091-7613(1975)3<232:cpbiga>2.0.co;2)
- Newhall, C. G. (1987). Geology of the Lake Atitlán region, western Guatemala. *Journal of Volcanology and Geothermal Research*, *33*, 23–55. [https://doi.org/10.1016/0377-0273\(87\)90053-9](https://doi.org/10.1016/0377-0273(87)90053-9)
- Phipps Morgan, J. P., Ranero, C. R., & Vannucchi, P. (2008). Intra-arc extension in Central America: Links between plate motions, tectonics, volcanism, and geochemistry. *Earth and Planetary Science Letters*, *272*, 365–371. <https://doi.org/10.1016/j.epsl.2008.05.004>
- Plafker, G. (1976). Tectonic aspects of the Guatemala Earthquake of February 4, 1976. *Science*, *193*(4259), 1202–1208. <https://doi.org/10.1126/science.193.4259.1201>
- Reynolds, J. H. (1977). *Tertiary volcanic stratigraphy of northern Central America*, (Masters thesis). Dartmouth College.
- Reynolds, J. H. (1980). Late Tertiary volcanic stratigraphy of northern Central America. *Bulletin of Volcanology*, *43*(3), 601–607. <https://doi.org/10.1007/bf02597696>
- Ritchie, A. W. (1975). *Geology of the San Juan Sacatepéquez quadrangle, Guatemala, Central America*, (Ph.d. dissertation, p. 132). University of Texas at Austin.
- Rodríguez, M., DeMets, C., Rogers, R., Tenorio, C., & Hernandez, D. (2009). A GPS and modeling study of deformation in northern Central America. *Geophysical Journal International*, *178*, 1733–1754. <https://doi.org/10.1111/j.1365-246x.2009.04251.x>
- Rogers, R. D., Karason, H., & van der Hilst, R. D. (2002). Epeirogenic uplift above a detached slab in northern Central America. *Geology*, *30*(11), 1031–1034. [https://doi.org/10.1130/0091-7613\(2002\)030<1031:euads>2.0.co;2](https://doi.org/10.1130/0091-7613(2002)030<1031:euads>2.0.co;2)
- Rogers, R. D., & Mann, P. (2007). *Transensional deformation of the western Caribbean-North America plate boundary zone* (Vol. 428, pp. 37–64). The Geological Society of America Special Paper.
- Rose, W. I., Conway, F. M., Pullinger, C. R., Deino, A., & McIntosh, W. C. (1999). An improved age framework for late Quaternary silicic eruptions in northern Central America. *Bulletin of Volcanology*, *61*, 106–120. <https://doi.org/10.1007/s004450050266>
- Rose, W. I., Grant, N. K., & Easter, J. (1979). *Geochemistry of the Los Chocoyos Ash, Quezaltenango Valley, Guatemala* (Vol. 180, pp. 87–99). Geological Society of America Special Paper. <https://doi.org/10.1130/spe180-p87>
- Rose, W. I., Hahn, G. A., Drexler, J. W., Malinicono, M. L., Peterson, P. S., & Wunderman, R. L. (1981). Quaternary tephra of northern Central America. In S. Self, & R. S. J. Sparks (Eds.), *Tephra studies, NATO Advanced Study Institutes Series (Series C—Mathematical and Physical Sciences)* (Vol. 75, pp. 193–211). Dordrecht, Springer. https://doi.org/10.1007/978-94-009-8537-7_11
- Rose, W. I., Newhall, C. G., Bornhorst, T. J., & Self, S. (1987). Quaternary silicic pyroclastic deposits of Atitlán Caldera, Guatemala. *Journal of Volcanology and Geothermal Research*, *33*, 57–80. [https://doi.org/10.1016/0377-0273\(87\)90054-0](https://doi.org/10.1016/0377-0273(87)90054-0)
- Sarna-Wojcicki, A. M. (2000). Tephrochronology. In J. S. Noller, J. M. Sowers, & W. R. Lettis (Eds.), *Quaternary geochronology: Methods and applications* (Vol. 4, pp. 357–377). Washington, DC: American Geophysical Union, AGU Reference Shelf Series.
- Sarna-Wojcicki, A. M., Bowman, H. R., Meyer, C. E., Russell, P. C., Woodward, M. J., McCoy, G., et al. (1984). *Chemical analyses, correlations, and ages of upper Pliocene and Pleistocene ash layers of East-Central and Southern California* (Vol. 1293, p. 22). Geological Survey Professional Paper.
- Saxby, J., Gottsmann, J., Cashman, K., & Gutiérrez, E. (2016). Magma storage in a strike-slip caldera. *Nature*, *7*, 12295. <https://doi.org/10.1038/ncomms12295>
- Schindlbeck, J. C., Kutterolf, S., Freundt, A., Eisele, S., Wang, K.-L., & Frische, M. (2016). Miocene to Holocene Marine tephrostratigraphy offshore northern Central America and southern Mexico: Pulsed activity of known volcanic complexes. *Geochemistry, Geophysics, Geosystems*, *19*, 4143–4173.
- Staller, A., Martínez-Díaz, J. J., Benito, B., Alonso-Henar, J., Hernández, D., Hernández-Rey, R., et al. (2016). Present-day crustal deformation along the El Salvador Fault Zone from ZFESNet GPS network. *Tectonophysics*, *670*, 66–81. <https://doi.org/10.1016/j.tecto.2015.12.017>
- Suñe-Puchol, I., Aguirre-Díaz, G. J., Dávila-Harris, P., Miggins, D. P., Pedrazzi, D., Costa, A., et al. (2019). The Ilopango caldera complex, El Salvador: Origin and early ignimbrite-forming eruptions of a graben/pull-apart caldera structure. *Journal of Volcanology and Geothermal Research*, *371*, 1–19.
- Titus, S. J., Housen, B., & Tikoff, B. (2007). A kinematic model for the Rinconada fault system in central California based on structural analysis of en echelon folds and paleomagnetism. *Journal of Structural Geology*, *29*, 961–982. <https://doi.org/10.1016/j.jsg.2007.02.004>
- Walsh, J., Watterson, J., & Yielding, G. (1991). The importance of small-scale faulting in regional extension. *Nature*, *351*, 391–393. <https://doi.org/10.1038/351391a0>
- Wang, S., Yu, H., Zhang, Q., & Zhao, Y. (2018). Absolute plate motions relative to deep mantle plumes. *Earth and Planetary Science Letters*, *490*, 88–99. <https://doi.org/10.1016/j.epsl.2018.03.021>
- Williams, H. (1960). *Volcanic history of the Guatemalan highlands* (Vol. 38, pp. 1–86). University of California Publications in Geological Sciences.
- Wunderman, R. L., & Rose, W. I. (1984). Amatitlán, an actively resurging cauldron 10 km south of Guatemala City. *Journal of Geophysical Research*, *89*(B10), 8525–8539. <https://doi.org/10.1029/jb089ib10p08525>
- Xu, S. S., Nieto-Samaniego, A. F., & Alaniz-Alvarez, S. A. (2009). Quantification of true displacement using apparent displacement along an arbitrary line on a fault plane. *Tectonophysics*, *467*, 107–118. <https://doi.org/10.1016/j.tecto.2008.12.004>
- Xu, S. S., Velasquillo-Martínez, L. G., Grajales-Nichimura, J. M., Murillo-Muñetón, G., & Nieto-Samaniego, A. F. (2007). Methods for quantitatively determining fault slip using fault separation. *Journal of Structural Geology*, *29*, 1709–1720. <https://doi.org/10.1016/j.jsg.2007.06.003>
- York, D. (1973). Evolution of triple junctions. *Nature*, *244*, 341–342. <https://doi.org/10.1038/244341a0>